Tsunami arrival time detection system applicable to discontinuous time-series data with outliers

Jun-Whan Lee [1], Sun-Cheon Park[1], Duk Kee Lee[1], Jong Ho Lee[1]

[1]National Institute of Meteorological Sciences, 33, Seohobuk-ro, Seogwipo-si, Jeju-do, 63568, Rep. of Korea

Correspondence to: Sun-Cheon Park (suncheon@korea.kr)

Abstract. Timely detection of tsunamis with water-level records is a critical but logistically challenging task because of outliers and gaps. Since tsunami detection algorithms require several hours of past data, outliers could cause false alarms and gaps can stop the tsunami detection algorithm even after the recording is restarted. In order to avoid such false alarms and time delays, we propose a tsunami arrival time detection system (TADS) that can be applied to discontinuous time-series data with outliers. The TADS consists of three algorithms, outlier removal, gap filling, and tsunami detection, which are designed to update whenever new data is acquired. After calibrating the thresholds and parameters for the Ulleung-do surge gauge located in the East Sea, Korea, the performance of TADS was discussed based on a one-year dataset with historical tsunamis and synthetic tsunamis. The results show that the overall performance of TADS is effective in detecting a tsunami signal superimposed on both the outliers and gaps.

1 Introduction

A tsunami is one of the most devastating natural phenomena caused by several events such as seaquakes, submarine landslides, subaerial landslides, volcanic eruptions, asteroid and comet impacts, and man-made explosions (Pugh and Woodworth, 2014). The eastern coast of the Korean Peninsula is not exempt from tsunamis because of the high tsunami energy concentration at the coast based on the peculiar topographic conditions of the East Sea where the Yamato rise strongly affects the propagation of tsunamis (Cho and Lee, 2013). A low probability exists for tsunamis to occur in the East Sea. However, if and when they do occur, they pose a high risk of damage to not only Korea but also to neighboring countries. For example, two tsunamis in 1983 and 1993, which originated near the western coast of Akita and Hokkaido, Japan, respectively, caused severe damage along the eastern coast of the Korean Peninsula (Fig. 1).

The Korea Meteorological Administration (KMA), as the government's meteorological organ, is responsible for issuing information on tsunamis. To monitor tsunamis, the KMA has operated a surge gauge (aerial ultrasonic type) at Ulleung-do since 1999. The Ulleung-do, located in the East Sea, plays a critical role in tsunami hazard mitigation of the Korean Peninsula because it can confirm the approach of tsunamis 30 minutes or more before they impact the eastern coast (Fig. 1). However, when the Tohoku, Japan tsunami occurred in 2011, even though a post analysis revealed it to be a small tsunami (less than 0.3 m), the KMA could not announce important properties of the tsunami such as its arrival time and wave height

in a press release because of its lack of a tsunami detection system (Yoon et al., 2012). In the aftermath of the Tohoku tsunami, the National Institute of Meteorological Sciences (NIMS), KMA has seen the necessity in the development of a tsunami detection system that automatically provides prompt notification.

Because of the infrequent occurrence of large tsunamis in the East Sea, an important technical requirement for detecting tsunamis using the Ulleung-do surge gauge is a sensitive tsunami detection algorithm. To detect a tsunami automatically, several tsunami detection algorithms have been developed around the world based on specific purposes and limitations. Mofjeld (1997) developed a deep-ocean assessment and reporting of tsunamis (DART) algorithm that uses a cubic polynomial fit to the data over the preceding three hours (Meinig et al., 2005). Several refinements to this algorithm have been proposed. Beltrami (2008) modified the DART algorithm based on the artificial neural networks (ANNs) to update the coefficients of every sampling interval. Because the DART algorithm does not provide information on tsunami height but only on arrival time, Beltrami (2011) extended the length of the interval between the actual and prediction times. Bressan and Tinti (2012) proposed a tsunami early detection algorithm (TEDA) designed to detect an anomalous water-level based on two slope-based algorithms: tsunami detection and secure detection. The TEDA was successfully calibrated and tested on both synthetic tsunamis and historical tsunami records (Bressan and Tinti, 2012; Bressan et al., 2013). Pérez et al. (2013) introduced a real-time automatic tsunami detection algorithm based on a variance method which was developed within the TRANSFER (Tsunami Risk And Strategies For the European Region) project. However, there was no attempt to combine several tsunami detection algorithms to not only detect weak tsunami signals but also to reduce the probability of false alarms.

The Ulleung-do surge gauge often experience unexpected gaps or missing points that cause major difficulties in detecting tsunamis. These difficulties are explained by such occurrences as: a failure of the recording or interruption of the communication network, aging equipment, and mistakes by field staff (Ustoorikar and Deo, 2008). When data are lost or incomplete, the tsunami detection algorithms that require several hours of data get stopped even after the recording is restarted. For long gaps that are expected to include complex patterns, any kinds of interpolation methods might not be suitable to fill the gaps. Thus, several kinds of soft computing techniques for long gaps have been developed. These include chaos theory, genetic programming, empirical orthogonal functions, and artificial neural networks (ANNs) (Elshorbagy et al., 2002; Nitsure et al., 2014; Tolkova, 2009; Pashova and Popova, 2011). Recently, Lee and Park (2016) developed a gap filling algorithm based on ANNs and an end-point fixing method (EPFM). Although the soft computing techniques are quite accurate, these applications require considerable computing time. In order to overcome these kinds of shortcomings, Lee and Park (2015) developed a gap filling algorithm which is similar to Lee and Park (2016)'s method but used a moving average filter rather than an ANNs. However, these methods mentioned above are unnecessarily complex for short gaps where linear change is expected so that a linear interpolation may be enough. Thus, in order to deal with gaps efficiently, a tsunami detection system requires a gap filling algorithm that applies different methods depending on the gap size.

Detecting tsunamis using the Ulleung-do surge gauge is logistically challenging because onshore measurements are usually associated with high background noise (Joseph, 2011). In addition, outliers derive from various problems related, for

example, to meteorological events or electrical malfunctions occurring in water-level sensor data streams (Fig. 2). When the outliers are mixed with normal data, the tsunami detection algorithms that require several hours of past data could cause a false alarm. Because outlier removal (as well as the anomaly detection, despiking, and noise removal) has been researched for a long time, various techniques have been developed. Ehrentreich and Sümmchen (2001) used a wavelet transform method to remove the spikes from the Raman spectra. Feuerstein et al. (2009) developed a despiking algorithm based on filtering methods using clinical data. Goring and Nikora (2002) and Jesson et al. (2013) presented a phase-space thresholding method that is applied to automated post-processing software to remove spikes from acoustic Doppler velocimeter data (Jesson et al., 2015). However, these methods require a complete set of data or data in a batch. Thus, they are not suitable for real-time or near real-time applications (Hill et al., 2009). To perform in real-time or near real-time, the outlier removal algorithm must consider the data stream sequentially or the outlier should be detected immediately after it appears. Several studies have defined a window that steps through the data stream to operate in real-time. The most up-to-date survey on the window-based outlier removal algorithm was provided by Gupta et al. (2014). Yamanishi and Takeuchi (2002) developed an on-line discounting learning algorithm that gradually forgets the effect of past data. Hill et al. (2009) developed an outlier removal algorithm based on dynamic Bayesian networks that adds new state variables over time. Hill and Minsker (2010) developed an outlier removal algorithm based on a data-driven univariate autoregressive model and corresponding prediction interval. However, most of these algorithms that predict the subsequent set of chronologically sequential data using soft computing techniques require huge memory and considerable computation time. Thus, the tsunami detection system requires an outlier removal algorithm which could obviate outliers very quickly within the time interval of data acquisition.

Overall, a tsunami detection system should be designed for the detection of a tsunami signal superimposed on both an outlier and gap. This study presents a tsunami detection system applicable to discontinuous time-series data with outliers, which we call TADS (Tsunami Arrival time Detection System). The 10-second interval data of the Ulleung-do surge gauge recorded from March 1–31, 2011 were employed to calibrate the parameters of TADS, in which not only outliers and gaps but also the 2011 Tohoku tsunami signals were included (Fig. 2). Outliers that may have resulted from meteorological events were found in similar periods identified in special weather reports. In addition, suspicious gaps lasting 6 hours were found in the data of the day before the 2011 Tohoku earthquake. After calibrating the parameters, the performance of TADS was demonstrated based on a one-year dataset with historical tsunamis and synthetic tsunamis.

2 TADS (Tsunami Arrival time Detection System)

TADS comprises basically of three major algorithms which are designed to operate within the time interval of data acquisition (Fig. 3). 1. Outlier removal algorithm (red dotted box) which is divided into three modes: start mode, keep mode, and end mode. 2. Gap filling algorithm (blue dotted box) which is divided into two sub-algorithms depending on gap sizes: SGFA (Short Gap Filling Algorithm) and LGFA (Long Gap Filling Algorithm). 3. Tsunami detection algorithm (green

dotted box) which is divided into three sub-algorithms: DART, SLOPE, and TIDE. And the alarm is divided into three levels depending on TDI (Tsunami Detection Index), a degree of tsunami detection triggered: warning, advisory, and watch.

Since most of the tsunami detection algorithm is designed to detect a wave that changes more than expected, the tsunami detection algorithm could not distinguish a tsunami from a record that may contain contributions from swells, local seiches, storm surges, and so on (Joseph, 2011). If the tsunami detection algorithm is applied to the data of the Ulleung-do surge gauge without any restriction, then the tsunami alarm will be issued for not only tsunamis but also for every event mentioned above. Also, even though the outlier removal and gap filling algorithms are useful for the tsunami detection system, these algorithms could distort a tsunami wave. The outlier removal algorithm could remove a tsunami wave by misunderstanding a tsunami wave as an outlier. And the gap filling algorithm could overestimate or underestimate a tsunami wave which could mislead to a false alarm. For these reasons, we introduced a concept of an event period that if the data comes under an event period, the TADS bypasses not only the outlier removal and gap filling algorithms but also the alarm of the tsunami detection algorithm. Since seaquakes are responsible for approximately 82% of tsunamis according to the tsunami database (Joseph, 2011), we confined the starting point of the event period to the origin time based on seismic information. On the other hand, the end point of the event period is set to the estimated time where a tsunami sufficiently elapses based on a numerical simulation. In the remainder of this section, the methodology of each algorithm will be described in detail. How the parameters of TADS are determined will be explained in the next session.

2.1 Outlier removal algorithm

An outlier removal algorithm performs one of the three modes at every new data acquisition. The initiation is set to the start mode, and it searches for the point at which the outlier begins based on several starting conditions. Once the outlier is detected, the outlier removal algorithm removes the outlier and changes the mode to the keep mode. The keep mode continues to remove the datum until meeting the predefined time steps. Then the mode is changed to the end mode which keeps removing the datum until satisfying one of the ending conditions. Once the ending condition is triggered, the mode returns to the start mode. The full process of modes and conditions are described below.

2.1.1 Start mode

The basic concept of the start mode is that the point at which the difference in wave height between neighboring points surpasses the threshold is designated as an outlier (Fig. 4a). In order to deal with gaps (which will be explained later), a moving window of the most recent 7-point data is defined in which each point is numbered in an ascending order from zero to six. Fig. 4a shows the case where point 3 and point 6 are gaps. The wave height and its time information of point are hereafter referred to as h and t with a subscript indicating the point number. The point 5 is a target point which determines whether the point is an outlier or not. In other words, the point 5 is designated as an outlier if the data within the moving window satisfies one of the starting conditions. For example, as shown in Fig. 4a, if the difference between h_2 and h_5 exceeds a given threshold TH2 (i.e. $h_2 - h_5 > \mathrm{TH2}$), then the target point (point 5) is considered as an outlier. The

information of the target point (sign S, wave height h_s and its timing t_s), which will be used in the end mode, is stored in memory. The sign S is based on a sign function of a real number x and can be expressed as:

$$\mathrm{sgn}(x) = \begin{cases} -1 & \text{if } x < 0, \\ 0 & \text{if } x = 0, \\ 1 & \text{if } x > 0. \end{cases} \quad (1)$$

The total starting conditions and the thresholds are listed in Table 1. The backgrounds and the details of each condition are described below. One common problem in the start mode is the presence of gaps in the data stream because the difference in wave height between neighboring points could not be calculated if a gap exists. For example, if point 3 is a gap, the difference in wave height between point 5 and point 3 could not be obtained. In order to deal with gaps, the start mode stores a wave height (h_g) of one point before the target point and counts the length of gaps (t_g) whenever the target point meets a gap (Fig. 4a). Also, the starting conditions are divided into two categories depending on whether point 6, one point before the target point, is a gap or not. SIF1 is the condition where point 6 is a gap while SIF2 is the condition where point 6 is not a gap. For SIF1, to catch an outlier which starts right after the gaps, the target point (point 5) is designated as an outlier if the absolute value of the difference between h_5 and h_g exceeds a given threshold THh (called S01). For SIF2, the target point is designated as an outlier if the difference between h_5 and the wave heights of the other points from point 0 to point 4 exceeds a given threshold assigned depending on not only the distance between points but also the sign of the water-level change. TH0, TH1, TH2, TH3, and TH4 are the thresholds for cases in which the sign of the difference between h_5 and the wave heights of the other points from the point 0 to the point 4 is a positive number (plus sign) or zero. By contrast, TH_0, TH_1, TH_2, TH_3 and TH_4 are the thresholds for the cases in which the sign of difference is a negative number (minus sign). The corresponding conditions are called S02 – S11. In summary, the start mode designates the target point as an outlier and is changed to keep the mode if one of the starting conditions (S01 – S11) is satisfied.

2.1.2 Keep mode

The intermediate points between two points triggered at start mode are always outliers. Thus, the keep mode obviates the unnecessary procedure of the start mode to determine whether the target point is an outlier or not for the intermediate points. The outlier removal algorithm keeps the keep mode for a certain time step depending on the thresholds which were triggered at the start mode: no time step for THh, TH4, TH_4; one-time step for TH3, TH_3; two-time step for TH2, TH_2; three-time step for TH1, TH_1; four-time step for TH0, TH_0. For example, as shown in Fig. 4a, if point 5 was designated as an outlier because the difference between h_2 and h_5 exceeded TH2 (i.e. $h_2 - h_5 >$ TH2) at the start mode, then the intermediate points, point 3 and point 4 in Fig. 4a (which became point 4 and point 5 in Fig. 4b), are designated as outliers at the keep mode. In other words, the outlier removal algorithm keeps removing the data for a two-time step (because the outlier was designated by TH2) and then changes the mode to the end mode.

2.1.3 End mode

The end mode continues to remove the data until satisfying one of the ending conditions combined with sub-conditions which is related to wave height, sign and time span. For example, as shown in Fig. 4c, the ending conditions are combinations of several sub-conditions such as the water-level retreats back to the normal water-level (e.g. $|h_s - h_5| \leq$ THS1) or the slope of the water-level is changed (e.g. $\mathrm{sgn}(h_6 - h_5) \neq$ S) or a quite long time passes by (e.g. $t_s - t_5 >$ THD1).

The total ending conditions and the thresholds are listed in Table 1. The backgrounds and the details of each condition are described below. Similar to the start mode, one common problem of the end mode is the presence of gaps in the data stream. In order to deal with gaps, the ending conditions divided into three categories depends on whether point 5 and point 6 are a gap or not. EIF1 is the condition where point 5 is a gap, EIF2 is the condition where not point 5 but point 6 is a gap, and EIF3 is the condition where both point 5 and point 6 are not a gap. For EIF1, if not only the sign is reversed with S ($\mathrm{sgn}(h_4 - h_6) \neq$ S or 0) but also the water-level retreats back to the normal water-level ($\mathrm{abs}(h_s - h_6) \leq$ THS1) then the algorithm stops removing the data (called E01). For EIF2, since point 5 is not a gap any more, a similar condition with E01 ($\mathrm{sgn}(h_4 - h_5) \neq$ S or 0 & $\mathrm{abs}(h_s - h_5) \leq$ THS1) is applied where point 5 is used instead of point 6 (called E02). For EIF3, the end mode stops if the sign is reversed from negative to positive (($\mathrm{sgn}(h_s - h_5) = -1$) & (S = -1)) or vice versa (($\mathrm{sgn}(h_s - h_5) = 1$) & (S = 1)) and these conditions are called E03, E04, respectively. Also, the end mode stops if not only a certain time passes ($t_s - t_5 >$ THD1) but also the water-level retreats back to the normal water-level ($\mathrm{abs}(h_s - h_5) \leq 1$) and this condition is called E05. If a quite long time passes by ($t_s - t_5 >$ THD2), more relaxed condition ($\mathrm{abs}(h_s - h_5) \leq 2$) than E05 is applied and this condition is called E06. Another ending condition is required to deal with long outliers because of the tide that changes the mean water-level. In other words, the end point of long outliers within flood tide or ebb tide would not retreat back to the normal water-level. Thus, in order to deal with long outliers, two ending conditions are introduced. One way is to stop the end mode if not only the sign is reversed with S ($\mathrm{sgn}(h_6 - h_5) =$ S) but also the water-level change abruptly ($\mathrm{abs}(h_6 - h_5) \geq$ THS2) even though water-level does not retreat back to the normal water-level yet ($\mathrm{abs}(h_s - h_5) \leq$ THS3), and this condition is called E07. Another way is to stop the end mode if all four consecutive water-levels do not retreat back to the normal water-level but under certain range (called E08). In order to deal with long gaps, if the outlier starts after long gaps ($t_g >$ THD1) and the water-level retreats back to the normal water-level ($\mathrm{abs}(h_s - h_5) <$ THS4), the end mode stops and this condition is called E09. In summary, the end mode stops removing the data and reverts to start mode if one of the ending conditions (E01 – E09) is satisfied.

2.2 Gap filling algorithm

Because the gap filling algorithm is activated after the outlier removal algorithm, not only the gaps of the original data but also the outliers removed by the outlier removal algorithm are subject to the gap filling algorithm. The first step is to count

the gap size n_{Gap}. Whenever a gap ends, the gap filling algorithm performs one of the sub-algorithms (SGFA and LGFA) depending on predefined criterion n_{LGFA}. If the gap exists but its size is smaller than n_{LGFA}, the SGFA is applied. If the gap size is greater than n_{LGFA}, the LGFA is applied. The full process of sub-algorithms and parameters are described below.

2.2.1 SGFA (Short Gap Filling Algorithm)

Depending on gap sizes, the SGFA is again divided into two categories: one point gap and short gaps (Fig. 5). For one point gap, the gap is replaced by the wave height just before the gap ($h(t_{gap}) = h(t_{gap}-1)$) where t_{gap} is the time of the gap. For short gaps ($1 < n_{Gap} < n_{LGFA}$), linear interpolation is applied to fill the gap. If we use only one point for the linear interpolation, the results could not fit well because of a temporary water-level fluctuation just before short gaps. Thus, the number of points before short gaps (N_inter) is used for the linear interpolation.

2.2.2 LGFA (Long Gap Filling Algorithm)

The LGFA is divided into three steps (Fig. 6). The first step is to filter out a background noise by applying a MAF (Moving Average Filter) that sets a time interval at mv_{LGFA} (Fig. 6a), and define a target window which consists of gaps, EP1, EP2 and target data. The EP1 is the end point just before where gaps start while the EP2 is the end point just after where gaps end. The target data will be used to look for the data suitable for filling the gap in the next step. The size of the target window is proportional to the gap size ($\mathrm{windowsize} \times (n_{Gap} + 2)$), where windowsize is a factor that determines the size of the window.

The second step is to find the most suitable data to fill the gaps (Fig. 6b). The LGFA hypothesizes that the gaps will follow the trend of the past water-level movement. Thus, the most suitable data for gaps is the data which shows the most similar trend with those of the target data. In order to find the most suitable data, search window and search data are set to the same size as the target window and the target data, respectively. The MAE (Mean Absolute Error) between the target data and the search data is calculated while the search window moves back over the length of m_{search} from the EP1. The m_{search} is proportional to the size of a target window ($\mathrm{npastdata} \times \mathrm{windowsize} \times (n_{Gap} + 2)$), where npastdata is a factor. The search window that shows minimum MAE is selected for gap filling.

The last step is to fill the gaps (Fig. 6c). The SW (Search Window) data, which is the remaining data of the search window after concealing the search data, are rebalanced by the EPFM (End Point Fixing Method) to keep the continuity of the time series. The EPFM fixes the first and last points of SW data to the EP1 and EP2 and linearly balances the intermediate data using the following equation:

$$H_{EP}(t) = H_{ori}(t) + \frac{b-a}{d}(t-c) + a \quad \text{for } c \le t \le c+d \tag{2}$$

where $H_{EP}(t)$ is the water-level after the EPFM is applied (red circle in Fig. 6c), $H_{ori}(t)$ is the water-level before the EPFM is applied (translucent red circle in Fig 6c), a is the difference between the start point of SW data and EP1, b is the difference

between the end point of SW data and EP2, c is the time of the start point of SW data, and d is the time span of SW data. Finally, the resulting data called, SWEP (Search Window End Point fixed) data replace the gaps.

2.3 Tsunami detection algorithm

Tsunami detection algorithm performs three parallel sub-algorithms, denoted by DART, SLOPE, and TIDE, during every new data acquisition. There are total 4 thresholds: TH_{DART} for DART, TH_{IS} and TH_{CF} for SLOPE, TH_{TIDE} for TIDE. If any kind of threshold is triggered, the TDI increments by one and lasts for a time interval t_{detect}. Thus, the TDI ranges from zero (all thresholds are not triggered) to four (all thresholds are triggered). The higher TDI is, the more likely a tsunami is detected. When the TDI is equal to 4, a warning alarm (red) is activated; when the TDI is equal to 3, an advisory alarm (orange) is activated; finally, when the TDI is equal to 2 or 1, a watch alarm (yellow) is activated. The full process of sub-algorithms and parameters are described below.

2.3.1 DART

The DART is an amplitude-based algorithm that uses a cubic polynomial fit to predict the water-level (Fig. 7a). The predicted water-level could be obtained by a cubic polynomial fit to the data stored over the preceding 3 h and 10 min and can be expressed as:

$$h_{DART}(t) = \sum_{i=0}^{3} \omega_i \bar{h_i} \left(t - 1 - \frac{300}{\Delta t} - i\frac{3600}{\Delta t} \right) \quad (3)$$

where h_{DART} is the predicted water-level, $\bar{h}$ is the 10-minute average of the measured water-level, Δt is a sampling interval expressed in seconds, and ω_i are the coefficients calculated by applying Newton's forward divided difference formula. The DART index (DI) is defined as the absolute value of the difference between the measured water-level and the predicted water-level ($DI(t) = |h(t) - h_{DART}(t)|$). The DART assumes that tsunami detection occurs when the DI surpasses the threshold, that is:

$$DI(t_{now}) \geq TH_{DART} \quad (4)$$

2.3.2 SLOPE

The SLOPE is a slope-based algorithm designed to detect a tsunami with an impulsive front (Fig. 7b). Using the same terminology as Bressan and Tinti (2011), the average slope $IS_T(t)$ is calculated by a least square fitting over the time interval $I_{IS}(t)$ of length t_{IS}. The $Tide_{uns}(t)$ is the average $IS_T(t)$ over time interval $I_{Tide}(t)$ of length t_{GTide} going back from the past time t_{GTide}. The tide slope estimation Tide(t) is calculated by averaging the $Tide_{uns}(t)$ over an interval length t_{sm}. Now, the detided instantaneous slope IS(t) could be obtained by subtracting the tide slope estimation from the average slope ($IS(t) = IS_T(t) - Tide(t)$). The background slope BS(t) is calculated by Eq. (5) over time interval $I_{BS}(t)$ of length t_{BS} going back from the past time t_G.

$$BS(t) = \text{standard deviation of } IS(t') \cdot \sqrt{2}; \quad t' \in I_{BS} \quad (5)$$

Finally, we could get the control function CF(t) which is a ratio of the absolute value of the detided instantaneous slope to the background slope (CF(t) = |IS(t)|/BS(t)). The SLOPE assumes that tsunami detection occurs when the absolute values of the detided instantaneous slope and the control function surpasses the thresholds, respectively, that is:

$$|\mathrm{IS}(t_{now})| \geq \mathrm{TH}_{\mathrm{IS}} \quad (6)$$

$$\mathrm{CF}(t_{now}) \geq \mathrm{TH}_{\mathrm{CF}} \quad (7)$$

2.3.3 TIDE

The TIDE is an amplitude-based algorithm that uses a harmonic analysis (Fig. 7c). The sampled data $h_s(t)$ is collected from the water-level data h(t) regularly spaced at an sampling interval t_{sample} over the preceding time t_{BP}. When the event period starts, the T_TIDE is activated to predict the tide data $h_{Tide}(t)$ over the period $t_{BP} + t_{FP}$. The T_TIDE is a classical harmonic analysis program that evaluates the tidal constituents (frequency, amplitude, phase, etc.). A detailed description can be found in Pawlowicz et al. (2002). The detided water-level data $h_{Detide}(t)$ are obtained by subtracting the tide data from the water-level data ($h_{Detide}(t) = h(t) - h_{Tide}(t)$). The average detided data $h_{Mean}(t)$ over the time interval t_{mean} that starts from the most recent data are then obtained. The Tide Index (TI) is defined as the difference between the detided water-level and the mean water-level ($TI(t) = h_{Detide}(t) - h_{Mean}(t)$). The TIDE assumes that tsunami detection occurs when the absolute value of TI surpasses the threshold, that is:

$$|\mathrm{TI}(t_{now})| \geq \mathrm{TH}_{\mathrm{TIDE}} \quad (8)$$

3 Calibration of TADS

In order to calibrate the TADS, the water-level data of the Ulleung-do surge gauge recorded from March 1–31, 2011 were employed. After calibrating several parameters and thresholds of algorithms, the event period, which starts when a seaquake occurs and lasts until a tsunami sufficiently passes by, was set to 8 hours after the 2011 Tohoku earthquake based on the results of a numerical simulation (Lee et al., 2015).

3.1 Calibration of outlier removal algorithm

Since several equivocal outliers are hardly distinguishable, we used the tide estimation predicted by the T_TIDE to calibrate the outlier removal algorithm. After setting the thresholds of the outlier removal algorithm to arbitrary values, we compared the outlier's removed data with the tide estimation. Whenever the outlier removal algorithm has failed to remove the data which shows a large discrepancy between the water-level data and the tide estimation, we modulated the thresholds. On the other hand, whenever the outlier removal algorithm removed the data which shows a small discrepancy between the water-level data and the tide estimation, we also modulated the thresholds. The above-mentioned process was repeated until the thresholds converged to a certain value. The resulting values of thresholds are listed in Table 1.

Fig. 8 shows nine examples of results obtained using the outlier removal algorithm based on the calibrated thresholds. Fig. 8a shows a case in which two types of outliers are clearly detected: one that slowly increases and gradually decreases, and another that sharply increases and suddenly decreases. Fig. 8b and c show cases in which the long-term outliers that offset the data are also perfectly detected. Fig. 8d and h present cases in which the long-term outliers with gaps are clearly detected, which allow the algorithm to manage the missing data. Fig. 8e shows the double outliers. Here, the second outliers appear immediately after the first outliers. Fig. 8f shows the meteorological outliers when a wind wave advisory was in effect for the far East Sea. Fig. 8g presents a case in which approximately 10 minutes of gaps exist in the data stream. It should be noted that the point immediately after gaps is classified as normal. Fig. 8i shows the instantaneously oscillating outliers that maintain for approximately 10 minutes. We should focus on the points classified as normal among outliers in Fig. 8a, e, and i that prevent long-term gaps because the performance of the gap filling algorithm (which will be explained later) is in inverse proportion to the gap size.

3.2 Calibration of gap filling algorithm

After calibrating the thresholds of the outlier removal algorithm, we calibrated the parameters of the gap filling algorithm that ensure the best performance for the Ulleung-do surge gauge data (Table 2). The N_inter, which is the number of points for linear interpolation, was set to two points because of two reasons: one point was insufficient to prevent the slope distortion provoked by temporary water-level fluctuation while a value greater than two points did not show notably different performance. To calibrate the remaining parameters, we intentionally omitted water-levels in some periods and ran the gap filling algorithm to predict the gaps which was intentionally omitted. Then, the predicted water levels of gaps and the water-level data which was intentionally omitted were compared. The above-mentioned process was repeated until the algorithm ensured the best performance where the MAE between the intentionally omitted data and the predicted data showed the smallest value. Thirty-four cases of gap sizes from 3 to 36 hours with 1-hour intervals, and 31 datasets from March 12, 2011 to March 29, 2011 with 50,000-second intervals were considered. Finally, criterion n_{LGFA}, the standard gap size to decide whether to apply SGFA or LGFA, was set to be 4 hours which is the maximum value within the boundary where the same performance between SGFA and LGFA is guaranteed.

Fig. 9 shows four examples of the results obtained with the LGFA. Table 3 provides the information of window and the MAE (Mean Absolute Error) between predicted data and measured datafor those four examples. After selecting the data of search window (gray line) which shows the most similar trends with those of the target data (black line), the SWEP data (blue line) were compared with the data intentionally omitted (red line). It should be noted that the EPFM improves the accuracy of prediction in most cases. For example, Fig. 9a and b show cases in which the target data and the search data are similar but the SW data are not fit with the data intentionally omitted. Because the EPFM enforces the end point of the SW data to match the end point of the measured data, the SWEP data shows a good agreement with the data intentionally omitted. However, as shown in Fig. 9c and d, the EPFM is less effective for the cases in which the end point of the SW data is similar to that of the data intentionally omitted. We should note that even though comparatively lower accuracy is obtained as the

gap size increases, because the longest gaps of the Ulleung-do surge gauge between March 1st and March 31st are approximately 6 hours, the LGFA performs reliably in alleviating the gap filling problem.

3.3 Calibration of tsunami detection algorithm

The parameters of the tsunami detection algorithm are listed in Table 4. The parameters of DART were calculated by applying Newton's forward divided difference formula for the case of 10-second interval data of the Ulleung-do surge gauge. The parameters of SLOPE were set to the same values of Bressan and Tinti (2011) which were tested with a sufficient number of samples. The parameters of TIDE were set to the values as the total computing time allows. For example, the sampling interval t_{sample} was set to 1 min to accelerate the calculation of harmonic analysis. Also, we assumed that the dataset of 10 days are enough for harmonic analysis (t_{BP} = 10 days) and the tsunami would not last longer than 2 days (t_{FP} = 2 days). Lastly, the averaging interval t_{mean} was set to 1 h to filter out the high frequency component.

After fixing the parameters, the thresholds of tsunami detection algorithm were calibrated based on the record of the 2011 Tohoku tsunami. Since there is no absolute standard of tsunami's arrival time, the thresholds should compromise with preciseness. As the thresholds are set to large values, the rate of false alarm would decrease while the rate of miss would increase, and vice versa. Thus, after setting the thresholds to arbitrary values, we modulated the thresholds within the range of values that do not cause any false alarm or miss the alarm by visual inspection.

Fig. 10 shows the part of the calibration process of tsunami detection algorithm. For the sake of simplicity, the threshold configuration (TH_{DART} = 5 cm, TH_{IS} = 0.01 cm/s, TH_{CF} = 4, TH_{TIDE} = 5 cm) will be collectively referred to as one which is a standard value of the normalized threshold. As the normalized thresholds increase, all kinds of detection rate decrease and all kinds of start time of detection increase. The detection rate of CF becomes zero when the normalized threshold is greater than 1.34 (Fig. 10b). For that reason, the warning alarm disappears when the normalized threshold is greater than 1.34 (Fig. 10d). Even though both IS and CF derive from the SLOPE, the detection rate of CF yields more sensitive results than does the detection rate of IS. By contrast, two amplitude-based algorithms (DART and TIDE) show similar patterns of both detection rate and start time of detection. We should note that if the normalized threshold is set to less than 0.4, one or more thresholds are triggered within 8 minutes, which thus represents a false alarm (Fig. 10c). By contrast, if the normalized threshold is set to greater than 1.06, the start time of warning alarm is 16 minutes or more, which is the moment when the steep fluctuation in the water level has already passed (Fig. 10e). Thus, to prevent both a false alarm and a missed alarm, the normalized threshold should be set in the range of 0.4 to 1.06. In this study, we set the normalized threshold to one.

4 Performance of TADS

The performance of TADS has been evaluated by using three types of data. First, the 2011 Tohoku tsunami data of the Ulleung-do surge gauge were used to investigate the overall performance based on the real tsunami record. Second, the water-level data of the Ulleung-do surge gauge recorded from January 1, 2011 to December 31, 2011 were used to

investigate the performance of the outlier removal and gap filling algorithms. Third, several synthetic tsunamis were used to demonstrate the performance of the tsunami detection.

4.1 2011 Tohoku tsunami

Fig. 11 illustrates the comprehensive results of TADS based on the calibrated thresholds, where the application to the 2011 Tohoku tsunami data of the Ulleung-do surge gauge is shown. Looking at the comprehensive results of TADS based on the calibrated thresholds, the outlier removal algorithm removes the outliers which appear a few minutes after the end of the event period. On the other hand, the abrupt water-level change measured twice approximately 19 h after the 2011 Tohoku earthquake was not designated as outliers. For these reasons, all thresholds except TH_{CF} were triggered for that moment outside the event period. However, we should note that the tsunami detection algorithm, which skips the alarm for the event period, prevents the occurrence of a false alarm.

The Ulleung-do surge gauge goes offline on March 10, 2011 at 03:10:00 and restarts the recording on March 10, 2011 at 09:29:00. Fortunately, the gaps were filled with the LGFA of the gap filling algorithm immediately after the gauge restarts the recording. It should be noted that the tsunami detection algorithm might miss the alarm without the gap filling algorithm if the gauge goes offline just before the 2011 Tohoku earthquake.

There are warning alarms which appear on March 11, 2011 at 14:58:30 (approximately 12 min after the 2011 Tohoku earthquake struck) and remain for approximately 15 min (Fig. 11a). And the watch alarm with intermittent advisory alarm follows the warning alarm. If we recall that the arrival time which could be recognized in the records by eye inspection is about 8 min (Fig. 10), the delay time of warning alarm is about 4 min, and it is quite acceptable for practical use.

Since the 2011 Tohoku tsunami was a tsunami caused by seaquake, the event period could be defined properly and the tsunami was well detected. However, tsunamis can result from submarine landslides, subaerial landslides, volcanic eruptions, atmospheric disturbances, asteroid and comet impacts, and man-made explosions (Pugh and Woodworth, 2014). And Korea has experienced meteo-tsunamis in both 2007 and 2008, which engulfed a part of the western coast of Korean Peninsula, causing two and nine casualties, respectively (Yoon et al., 2014). Thus, future studies should attempt to link the event period with the information related to landslides, volcanic activity, and atmospheric pressure to cope with several types of tsunamis.

4.2 Performance of outlier removal and gap filling algorithms

Fig. 12 shows the results of outlier removal and gap filling algorithms based on the calibrated thresholds. It is observed that most of the conspicuous outliers which are related to meteorological events are well removed. This could be also checked by comparing the scatter plots where most of the outliers that stand out from the majority of the data are removed and the correlation increases after applying the algorithms. However, due to the outliers which remain inside a batch of outliers, it is seen that the SGFA (blue line in Fig. 12) fails to fill short gaps in a few cases. The LGFA (red line in Fig. 12) successfully fills long gaps following the trend of the tide estimation except in the case of May where the gaps appear in front of constant

water-level data sustained by an unknown reason. Since the target data are constant water-level data for this case, the results of LGFA shows the same results with those of the linear interpolation.

Of course, it is always possible that some outliers remain or gaps are not correctly filled. However, it should be noted that both the outlier removal algorithm and the gap filling algorithm significantly reduce the chance of discontinuous data with outliers entering the tsunami detection algorithm, the main objective of these developments.

4.3 Performance of tsunami detection algorithm

In order to investigate the performance of the tsunami detection algorithm, the algorithm should be tested based on an extensive number of tsunamis. However, the 2011 Tohoku tsunami is the only case which was recorded in the Ulleung-do surge gauge. For stations having insufficient tsunami records, Beltrami and Risio (2011) examined their tsunami detection algorithm with synthetic tsunami signals in which ideal sinusoidal tsunamis were superimposed on ideal wind-waves based on Jonswap wave-spectra. In addition, Bressan et al. (2013) tested their tsunami detection algorithm with synthetic tsunami signals in which the results of numerical simulation were superimposed on the tide gauge record of possible circumstances (e.g., calm or rough sea). Risio and Beltrami (2014) estimated the performance of the tsunami detection algorithm with historical tsunami signals, in which the record of the DART buoy was superimposed on the wind wave, which in turn was synthesized by means of the random-phase method. Thus, we introduced several synthetic tsunamis to demonstrate the performance of the tsunami detection.

The historical tsunamis that occurred on the 1983 Akita tsunami (M_w 7.8) and the 1993 Hokkaido tsunami (M_w 7.7) were recorded in several tide stations operated by the Korea Hydrographic and Oceanographic Agency (KHOA). Among the records, three records of the tide stations were selected which are well-preserved so that continuous records could be obtained. One is the record of the Ulleung-do tide station in 1983, and others are the records of the Ulleung-do and the Pohang tide stations in 1993. Also, even though the amplitude was very small, the 2011 Tohoku tsunami were recorded in several tide stations. We selected two records of tide stations, Tongyeong and Seongsanpo, which were recorded continuously. The location of tide stations could be found in Fig. 1.

For tsunami detection algorithm, one of the important performance indicators is the delay time between the actual arrival time and the time of the first alarm. In order to investigate the delay time, we set the standard arrival time to the arrival time records in the report on tsunami occurrence (KHOA, 2015). However, if the original records are applied to the tsunami detection algorithm directly, it is hard to investigate the delay time correctly because of the false alarm caused by the background records which are all different depending on the specific local characteristics. Thus, after extracting the tsunami records by detiding the original records, the tsunami records of 24 h were superimposed on the background records of the Ulleung-do surge gauge. The resulting time-series with the alarm level (red, orange, and yellow) are illustrated in Fig. 13. The records of the Ulleung-do tide station shows a similar trend with the 2011 Tohoku tsunami record of the Ulleung-do surge gauge where the amplitude relented after the tsunami has arrived (Fig. 13a-b). On the other hands, the records of the Pohang, Tongyeong and Seongsanpo tide stations oscillate consistently (Fig. 13c-e). In general, one could expect that the

larger the tsunami amplitude during the same time period, the shorter the delay time is. Indeed, the delay time was shorter than about 5 min for the records of the historical tsunamis (Fig. 13a-c), while the delay time was longer than about 10 min for the records of the 2011 Tohoku tsunami (Fig. 13d-e). Because of the small amplitude, the record of the Tongyeong tide station shows the warning alarm (red vertical line) at about 9 h after the arrival time, and the record of the Seongsanpo tide station shows no warning alarm. However, it should be noted that the tsunami detection algorithm detects a weak tsunami which is hard to be distinguished by visual inspection.

For further investigation of the relationship between the first wave slope and the delay time, 100 cases of synthetic tsunami records were built. The detided tsunami records were multiplied by the factor changing from 0.1 to 2.0 with 0.1 intervals, and then the records were superimposed on the background records. Fig. 14 shows the delay times of each alarm level (red, orange and yellow) against the first wave slope of all 100 cases. The first wave slope was defined as the rate of the change in the water level between the point of arrival time and the local maximum point which appears after the arrival time with respect to time. As we expected, the distribution shows that the first wave slope and the delay time are in inverse proportion. If the first wave slope is less than about 0.15 cm/min, which is the cases of tsunamis that arrive with slowly increasing waves, the tsunami detection algorithm could not issue the warning alarm for any case. However, it should be noted that the tsunami detection algorithm ensures the performance where the first wave slope larger than 1 cm/min could be alarmed within 10 min. In other words, the results show that the tsunami detection algorithm could detect a tsunami whose amplitude is larger than 10 cm within 10 minutes.

5 Conclusion

In the present study, we proposed a tsunami arrival time detection system (TADS) applicable to discontinuous time-series data with outliers. In order to avoid false alarms and time delays, the TADS comprises three major algorithms: outlier removal, gap filling, and tsunami detection. The outlier removal algorithm is designed to remove outliers very quickly within the time interval of data acquisition. The gap filling algorithm is designed to fill gaps efficiently by applying different methods depending on the gap size. The tsunami detection algorithm is designed to not only detect weak tsunamis but also to reduce false alarms by combining several algorithms.

The TADS has recognized the tsunami within a few minutes after its arrival for the 2011 Tohoku tsunami record of the Ulleung-do surge gauge. And the application of TADS to the one year dataset and synthetic tsunamis proved that the overall performance of TADS is effective at detecting a tsunami signal superimposed on both the outliers and gaps. We expect that the efficiency and simplicity of TADS enable its wide application in tsunami monitoring areas such as a support tool that averts calamity by providing a rapid confirmation of tsunami generation.

Acknowledgments

This study was supported by the "Research and Development for KMA Weather, Climate and Earth System Services" project of the National Institute of Meteorological Sciences.

References

Beltrami, G. M.: An ANN algorithm for automatic, real-time tsunami detection in deep-sea level measurements, Ocean Eng., 35, 572-587, 2008.

Beltrami, G. M.: Automatic, real-time detection and characterization of tsunamis in deep-sea level measurements, Ocean Eng., 38, 1677-1685, 2011.

Bressan, L. and Tinti, S.: Structure and performance of a real-time algorithm to detect tsunami or tsunami-like alert conditions based on sea-level records analysis, Nat. Hazards Earth Syst. Sci., 11, 1499-1521, 2011.

Bressan, L. and Tinti, S.: Detecting the 11 March 2011 Tohoku tsunami arrival on sea-level records in the Pacific Ocean: application and performance of the Tsunami Early Detection Algorithm (TEDA), Nat. Hazards Earth Syst. Sci., 12, 1583-1606, 2012.

Bressan, L., Zaniboni, F., and Tinti, S.: Calibration of a real-time tsunami detection algorithm for sites with no instrumental tsunami records: application to stations in Eastern Sicily, Italy, Nat. Hazards Earth Syst. Sci., 1, 2455-2493, 2013.

Cho, Y.-S. and Lee, J.-W.: Hazard Map with Probable Maximum Tsunamis, in: Proceedings of the 23th International Offshore and Polar Engineering Conference, Alaska, USA, 30. June-5. July 2013, 82-85, 2013.

Ehrentreich, F. and Sümmchen, L.: Spike removal and denoising of Raman spectra by wavelet transform methods, Anal. Chem., 73, 4364-4373, 2001.

Elshorbagy, A., Simonovic, S. P., and Panu, U. S.: Estimation of missing streamflow data using principles of chaos theory, J. Hydrol., 255, 123-133, 2002.

Feuerstein, D., Parker, K. H. and Boutelle, M. G.: Practical methods for noise removal: applications to spikes, nonstationary quasi-periodic noise, and baseline drift, Anal. Chem., 81, 4987-4994, 2009.

Goring, D. G. and Nikora, V. I.: Despiking acoustic Doppler velocimeter data, J. Hydraul. Eng., 128, 117-126, 2002.

Gupta, M., Gao, J., Aggarwal, C., and Han, J.: Outlier detection for temporal data: a survey, IEEE Transactions on Knowledge & Data Engineering, 26, 2250-2267, 2014.

Hill, D. J. and Minsker, B. S.: Anomaly detection in streaming environmental sensor data: A data-driven modeling approach, Environ. Model. Softw., 25, 1014-1022, 2010.

Hill, D. J., Minsker, B. S., and Amir, E.: Real-time Bayesian anomaly detection in streaming environmental data, Water Resour. Res., 45, 1-16, 2009.

Jesson, M., Sterling, M., and Bridgeman, J.: Despiking velocity time-series—Optimisation through the combination of spike detection and replacement methods, Flow Meas. Instrum., 30, 45-51, 2013.

Jesson, M. A., Bridgeman, J., and Sterling, M.: Novel software developments for the automated post-processing of high volumes of velocity time-series, Adv. Eng. Software, 89, 36-42, 2015.

Joseph, A.: Tsunamis: Detection, Monitoring, and Early-Warning Technologies, Academic Press, San Diego, USA, 2011.

Korea Hydrographic and Oceanographic Agency: The occurrence of tsunamis: analysis of tsunami records, Oceanic Abnormal Phenomena Report, Busan, Korea, 2015.

Lee, J.-W. and Park, S.-C.: Development of a gap-filling algorithm applicable to a tsunami warning system, in: Proceedings of the 25th International Ocean and Polar Engineering Conference, Hawaii, USA, 21-26 June 2015, 860-864, 2015.

Lee, J.-W. and Park, S.-C.: Artificial Neural Network-Based Data Recovery System for the Time Series of Tide Stations, J. Coastal Res., 32, 213-224, 2016.

Lee, J.-W., Park, S.-C., and Park, E. H.: Analysis of arrival time of the 2011 Tohoku, Japan Earthquake and tsunami measured in Korea, in: Proceedings of Earthquake Engineering Society of Korea Fall Conference, Jeju-do, Korea, 10-12 September 2015, 143-144, 2015.

Lee, J.-W., Park, S.-C., Lee, W.-J., and Lee, D. K.: Development of outlier detection algorithm applicable to a Korean surge-gauge, EGU General Assembly, Vienna, Austria, 17-22 April 2016, EGU2016-5324, 2016.

Meinig, C., Stalin, S. E., Nakamura, A. I., and Milburn, H. B.: Real-time deep-ocean tsunami measuring, monitoring, and reporting system: The NOAA DART Ⅱ description and disclosure, Oceans 2005 MTS/IEEE, Washington, DC, 2005.

Mofjeld, H. O.: Tsunami detection algorithm, http://www.ndbc.noaa.gov/dart/algorithm.shtml (last access: 29 April 2016), 1997.

Nitsure, S. P., Londhe, S. N., and Khare, K. C.: Prediction of sea water levels using wind information and soft computing techniques, Appl. Ocean Res., 47, 344-351, 2014.

Pashova, L. and Popova, S.: Daily sea level forecast at tide gauge Burgas, Bulgaria using artificial neural networks. J. Sea Res., 66, 154-161, 2011.

Pawlowicz, R., Beardsley, B., and Lentz, S.: Classical tidal harmonic analysis including error estimates in MATLAB using T_TIDE. Comput. Geosci., 28, 929-937, 2002.

Pelinovsky, E., Didenkulova, I., Mendez, F., Rybski, D. and Tinti, S.: Sea hazards. Nat. Hazards Earth Syst. Sci., 13, 1063-1067, 2013.

Pérez, B., Á lvarez Fanjul, E., Pérez, S., de Alfonso, M., and Vela, J.: Use of tide gauge data in operational oceanography and sea level hazard warning systems. J. Oper. Oceanogr., 6, 1-18, 2013.

Pugh, D. and Woodworth, P.: Sea-Level Science: Understanding Tides, Surges, Tsunamis and Mean Sea-Level Changes, Cambridge University Press, Cambridge, UK, 2014.

Risio, M. D. and Beltrami, G. M.: Algorithms for automatic, real-time tsunami detection in wind-wave measurements: using strategies and practical aspects, Procedia Eng., 70, 545-554, 2014.

Tolkova, E.: Principal component analysis of tsunami buoy record: Tide prediction and removal, Dyn. Atmos. Oceans, 46, 62-82, 2009.

Ustoorikar, K. and Deo, M. C.: Filling up gaps in wave data with genetic programming, Mar. struct., 21, 177-195, 2008.

Yamanishi, K. and Takeuchi, J. I.: A unifying framework for detecting outliers and change points from non-stationary time series data, in: Proceedings of the 8th ACM SIGKDD international conference on Knowledge discovery and data mining, Alberta, Canada, 23-26 July 2002, 676-681, 2002.

Yoon, S. B., Baek, U., Park, W. K., and Bae, J.S.: Practical forecast-warning system for distant tsunamis, J. Korea Water Resour. Assoc., 45, 997-1008, 2012.

Yoon, S. B., Shin, C. H. and Bae, J. S.: Analysis of Generation and Amplification Mechanism of Abnormal Waves Occurred along the West Coast of Korea, J. Korean Soc. Coastal Ocean Eng., 26, 314-326, 2014.

Table 1. Conditions and thresholds of an outlier removal algorithm.

Mode	Category	Condition Name	Condition	Threshold Name	Threshold
Start	SIF1		(h_6 = NaN)		
		S01.	abs($h_5 - h_g$) > THh	THh	7 cm
	SIF2		($h_6 \neq$ NaN)		
		S02.	(sgn(h_4- h_5) $\geq$ 0) & (h_4- h_5 > TH4)	TH4	3 cm
		S03.	(sgn(h_4- h_5) < 0) & (h_4- h_5 < -TH_4)	TH_4	3 cm
		S04.	(sgn(h_3- h_5) $\geq$ 0) & (h_3- h_5 > TH3)	TH3	3 cm
		S05.	(sgn(h_3- h_5) < 0) & (h_3- h_5 < -TH_3)	TH_3	9 cm
		S06.	(sgn(h_2- h_5) $\geq$ 0) & (h_2- h_5 > TH2)	TH2	3 cm
		S07.	(sgn(h_2- h_5) < 0) & (h_2- h_5 < -TH_2)	TH_2	10 cm
		S08.	(sgn(h_1- h_5) $\geq$ 0) & (h_1- h_5 > TH1)	TH1	4 cm
		S09.	(sgn(h_1- h_5) < 0) & (h_1- h_5 < -TH_1)	TH_1	10 cm
		S10.	(sgn(h_0- h_5) $\geq$ 0) & (h_0- h_5 > TH0)	TH0	4 cm
		S11.	(sgn(h_0- h_5) < 0) & (h_0- h_5 < -TH_0)	TH_0	10 cm
End	EIF1		(h_5 = NaN)		
		E01.	(sgn(h_4- h_6) $\neq$ S or 0) & (abs(h_s- h_6) $\leq$ THS1)	THS1	2 cm
	EIF2		($h_5 \neq$ NaN) & (h_6 = NaN)		
		E02.	(sgn(h_4- h_5) $\neq$ S or 0) & (abs(h_s- h_5) $\leq$ THS1)		
	EIF3		($h_5 \neq$ NaN) & ($h_6 \neq$ NaN)		
		E03.	(sgn(h_s- h_5) = -1) & (S = -1)		
		E04.	(sgn(h_s- h_5) = 1) & (S = 1)		
		E05.	(abs(h_s- h_5) $\leq$ 1) & (t_s- t_5 > THD1)	THD1	10 points
		E06.	(abs(h_s- h_5) $\leq$ 2) & (t_s- t_5 > THD2)	THD2	20 points
		E07.	(sgn(h_6- h_5) = S) & (abs(h_6- h_5) $\geq$ THS2) & (abs(h_s- h_5) $\leq$ THS3)	THS2 THS3	3 cm 5 cm
		E08.	(abs(h_s- h_2) $\leq$ THS3) & (abs(h_s- h_3) $\leq$ THS3) & (abs(h_s- h_4) $\leq$ THS3) & (abs(h_s- h_5) $\leq$ THS3)		
		E09.	(t_g > THD1) & (abs(h_s- h_5) < THS4)	THS4	2 cm

Table 2. Parameters of a gap filling algorithm.

Algorithm	Parameter	Value	Description
	n_{LGFA}	4 h	Standard gap size whether to apply SGFA or LGFA
SGFA	N_inter	2 points	Number of points from the last point before the gap
LGFA	mv_{LGFA}	10 min	Time interval which is used to calculate the moving-averaged data
	windowsize	2	Factor to determine the size of target window
	npastdata	100	Factor to determine the size of past dataset, m_{search}

Table 3. Examples of a gap filling algorithm. The information of window and the Mean Absolute Error (MAE) between the predicted data and measured data are listed.

Gap Size (hr)	Time of Starting Point		MAE (cm)
	Target Window	Search Window	
3	Mar. 31, 2011 05:31:10	Mar. 20, 2011 07:26:20	0.58
12	Mar. 21, 2011 21:07:10	Mar. 19, 2011 07:55:10	2.08
24	Mar. 17, 2011 15:21:40	Mar. 03, 2011 16:19:10	3.22
36	Mar. 21, 2011 15:36:00	Mar. 18, 2011 01:26:20	4.56

Table 4. Parameters and thresholds of a tsunami detection algorithm.

Algorithm	Parameter / Threshold	Value	Description
DART	ω_0	2.1957	Coefficient calculated by Newton's forward divided difference formula
	ω_1	-2.2038	Coefficient calculated by Newton's forward divided difference formula
	ω_2	1.3233	Coefficient calculated by Newton's forward divided difference formula
	ω_3	-0.3152	Coefficient calculated by Newton's forward divided difference formula
	TH_{DART}	5 cm	Threshold for the detection condition of DART: $DI(t_{now}) \geq TH_{DART}$
SLOPE	t_{IS}	10 min	Time interval used to compute the instantaneous slope, $IS_T(t)$
	t_{Tide}	1 h	Time interval used to compute the tide slope estimation, $Tide_{uns}(t)$
	t_{GTide}	16 min	Gap time to make $Tide_{uns}(t)$ independent from an incoming anomalous wave
	t_{sm}	6 min	Time interval to reduce oscillations of the tidal slope due to long period waves
	t_{BS}	1 h	Time interval which is used to calculate the background slope signal, BS(t)
	t_G	15 min	Delay time to reduce the correlation between IS(t) and BS(t)
	TH_{IS}	0.01 cm/s	Threshold for the detection condition of SLOPE: $\lvert IS(t_{now})\rvert \geq TH_{IS}$
	TH_{CF}	4	Threshold for the detection condition of SLOPE: $CF(t_{now}) \geq TH_{CF}$
TIDE	t_{sample}	1 min	Sampling interval to compute the tide estimation, $h_{Tide}(t)$
	t_{BP}	10 days	Time interval of past data used to compute the tide estimation, $h_{Tide}(t)$
	t_{FP}	2 days	Time interval used to predict the tide estimation, $h_{Tide}(t)$
	t_{mean}	1 h	Time interval used to compute the average detided data, $h_{Mean}(t)$
	TH_{TIDE}	5 cm	Threshold for the detection condition of TIDE: $\lvert TI(t_{now})\rvert \geq TH_{TIDE}$
	t_{detect}	10 min	Duration time of detection

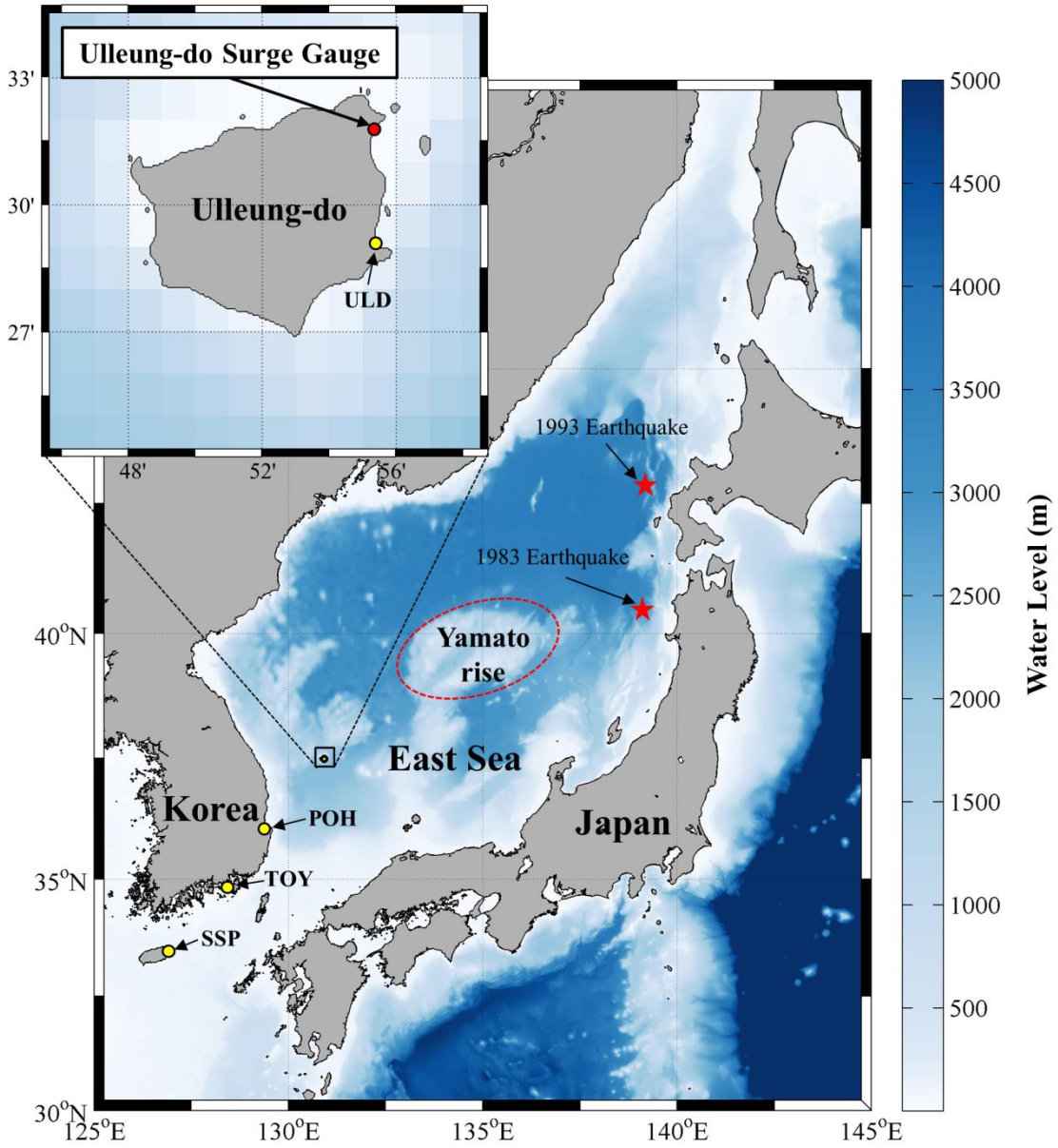

Figure 1: Study area and locations of the Ulleung-do surge gauge (red circle), tide stations (yellow circles), Yamato rise (red dotted circle), and the epicenters of the 1983 and 1993 earthquakes (red stars).

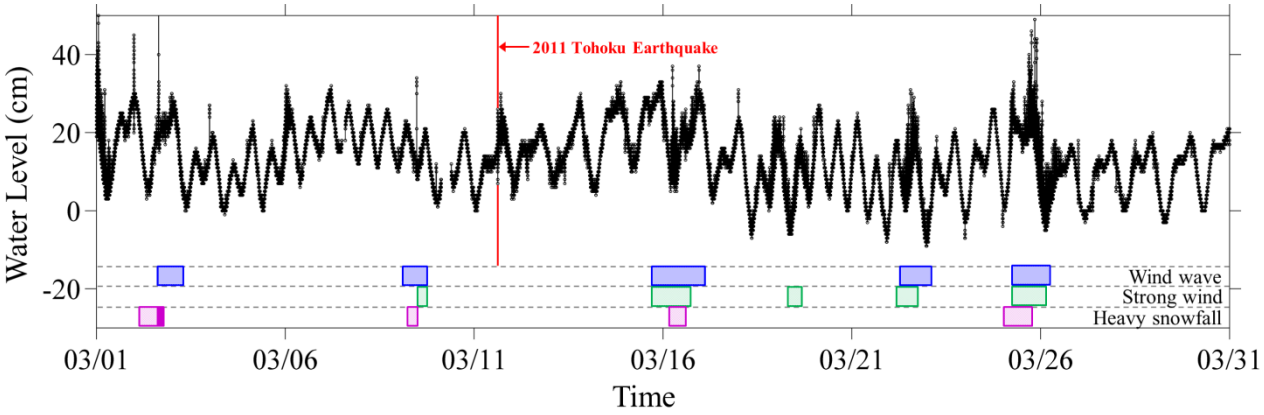

Figure 2: Time-series of the Ulleung-do surge gauge with a special weather report from the Korea Meteorological Administration (KMA). The dotted rectangles represent the following advisories: wind wave (blue), strong wind (green), and heavy snow (purple). The filled rectangle represents a heavy snow warning (purple). The red vertical line labeled "2011 Tohoku Earthquake" denotes the time of the earthquake.

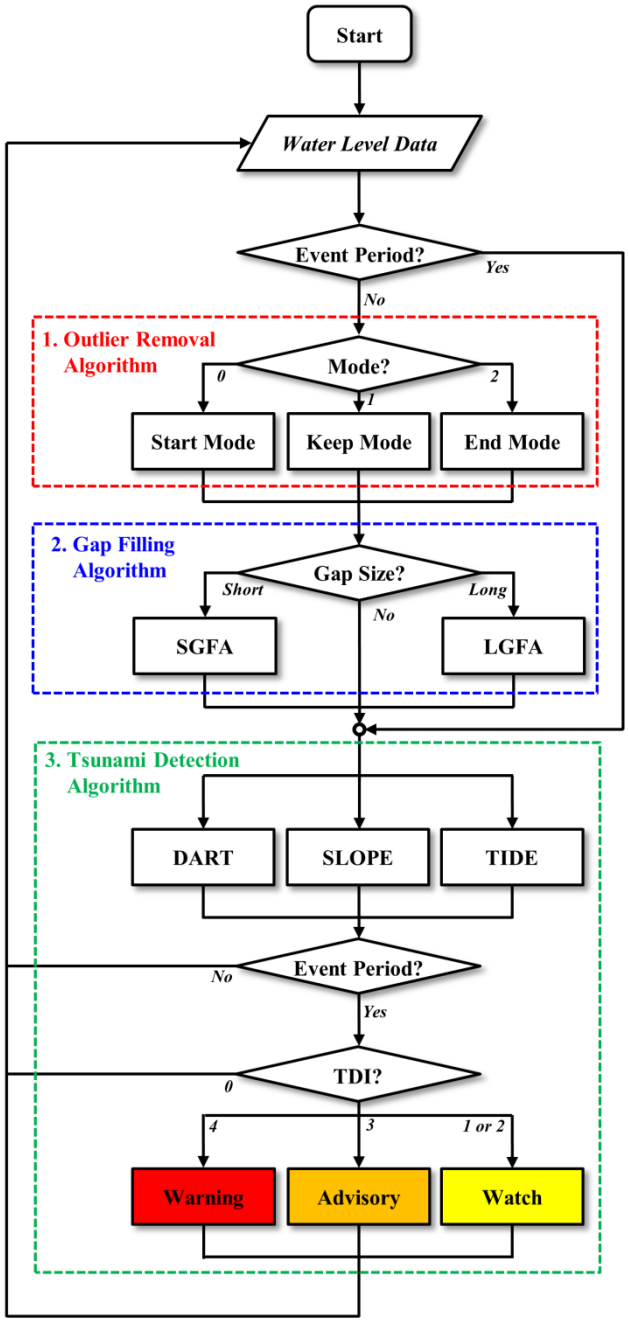

Figure 3: Flow of the TADS (Tsunami Arrival time Detection System). The system is composed of three major algorithms: outlier removal (red dotted box), gap filling (blue dotted box) and tsunami detection (green dotted box). SGFA stands for Short Gap Filling Algorithm; LGFA stands for Long Gap Filling Algorithm; TDI stands for Tsunami Detection Index.

5

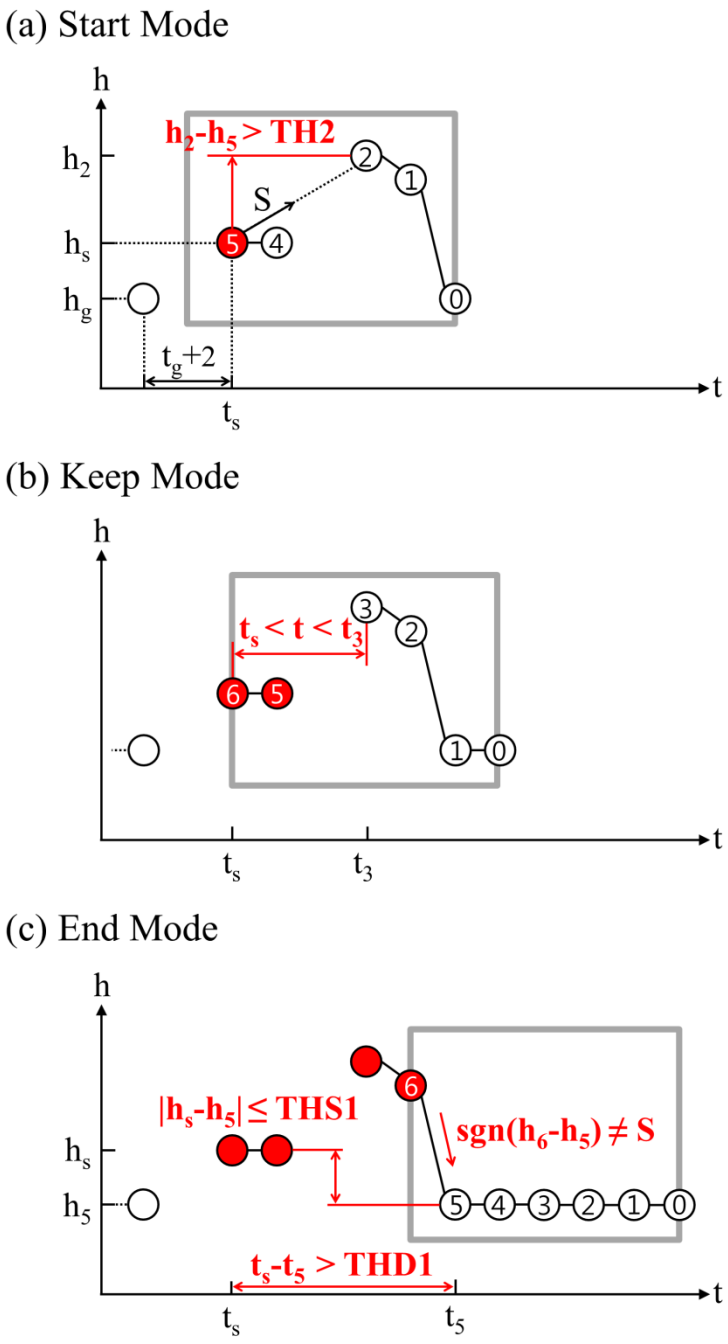

Figure 4: Schematic sketch of each mode of the outlier removal algorithm: (a) start mode, (b) keep mode, (c) end mode. The water-level data are represented as circles and a gray box indicates the moving window. Red circles indicate detected outliers and conditions are written in red.

5

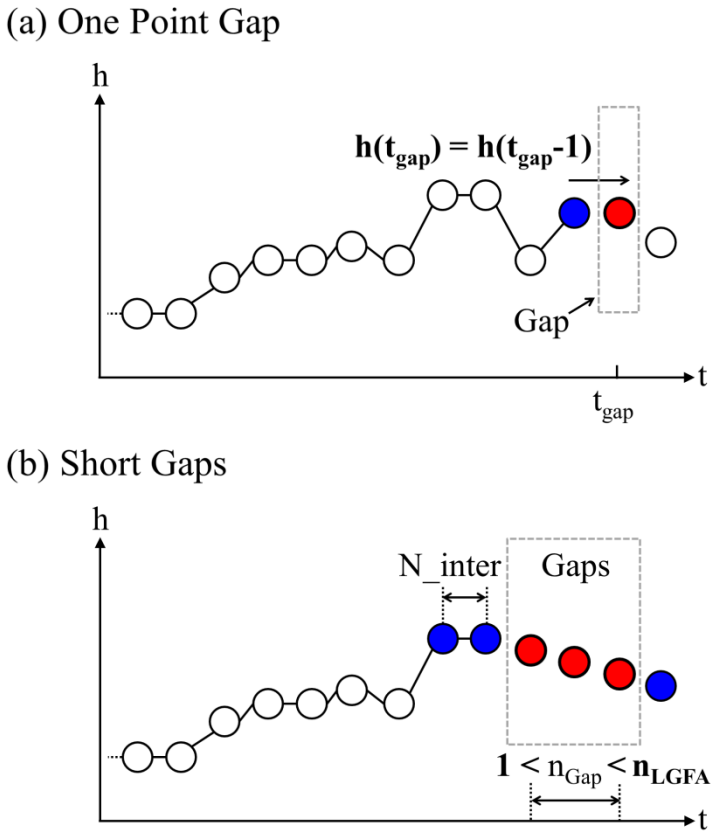

Figure 5: Schematic sketch of SGFA of the gap filling algorithm: (a) one point gap, (b) short gaps. The water-level data are represented as circles and a gray dotted box indicates the location of gaps. Blue circles indicate the data used to fill the gaps and red circles indicate gap-filled data.

5

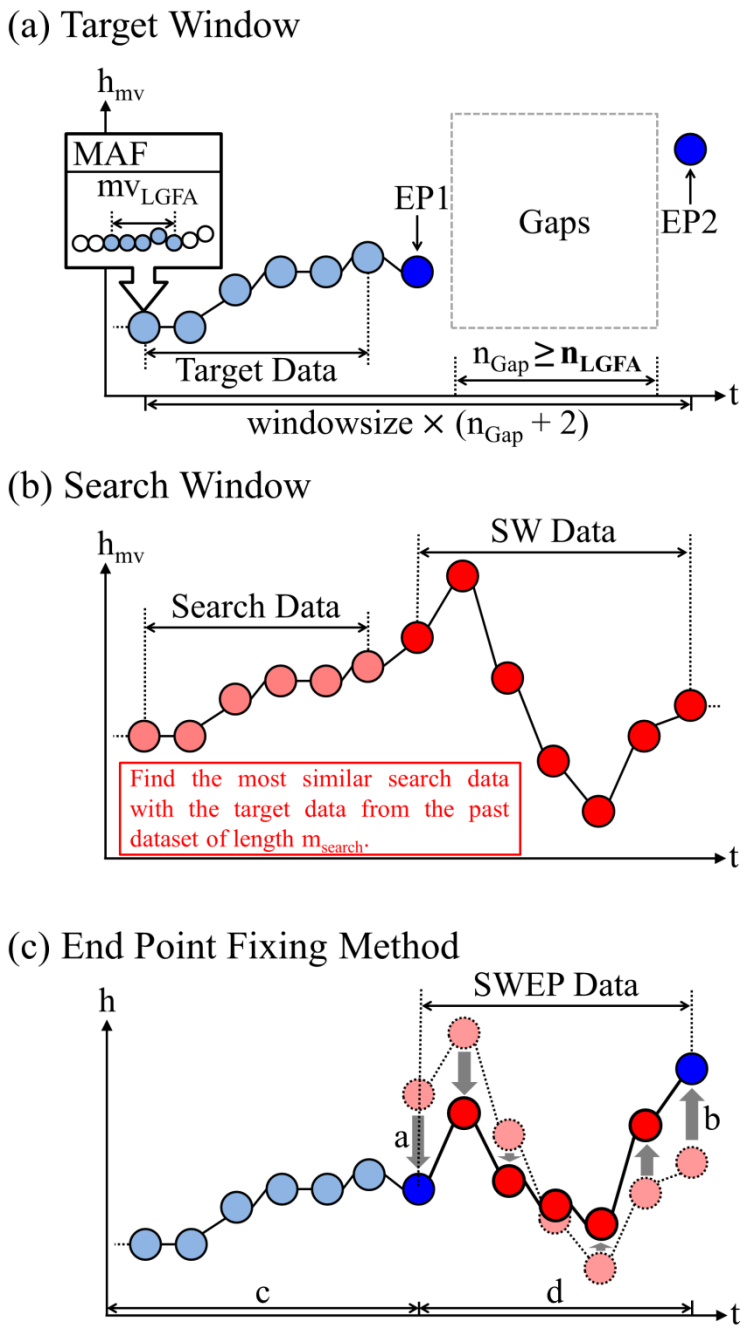

Figure 6: Schematic sketch of LGFA of the gap filling algorithm: (a) target window (blue tone), (b) search window (red tone), (c) end point fixing method. The water-level data are represented as circles and a gray dotted box indicates the location of gaps. MAF stands for Moving Average Filter. The moving averaged data are referred to as h_{mv}.

5

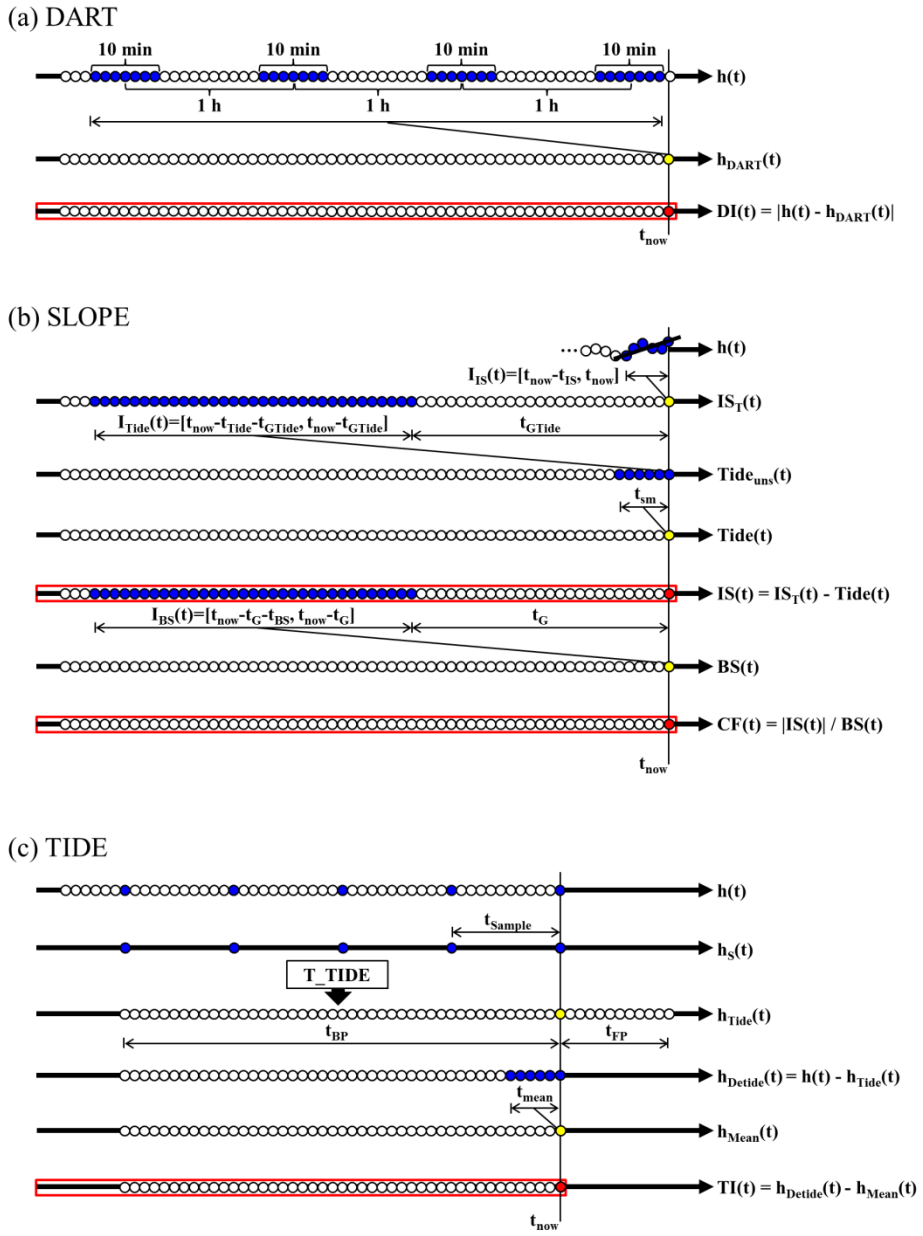

Figure 7: Schematic sketch of the tsunami detection algorithm: (a) DART, (b) SLOPE, (c) TIDE. From top bottom: the procedures of how the indexes, DI, IS, CF and TI (red boxes), are calculated from the water-level data. Each index (red circle) is calculated using the past data (blue circles) and the intermediate outputs (yellow circles) whenever new data is acquired.

5

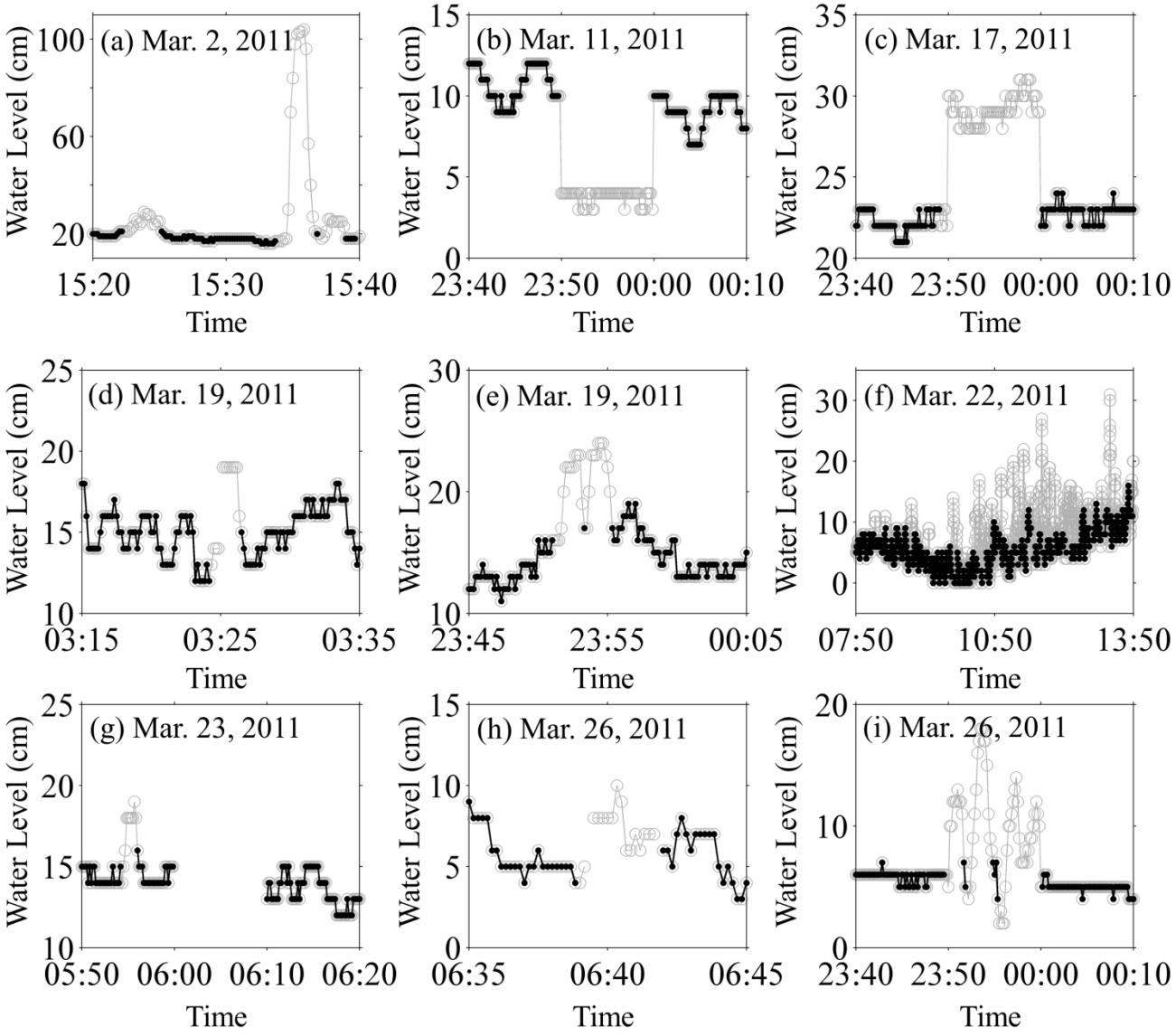

Figure 8: Examples of an outlier removal algorithm using calibrated thresholds. The gray line with a circle represents the original data, and the black line with a circle represents the outlier-removed data.

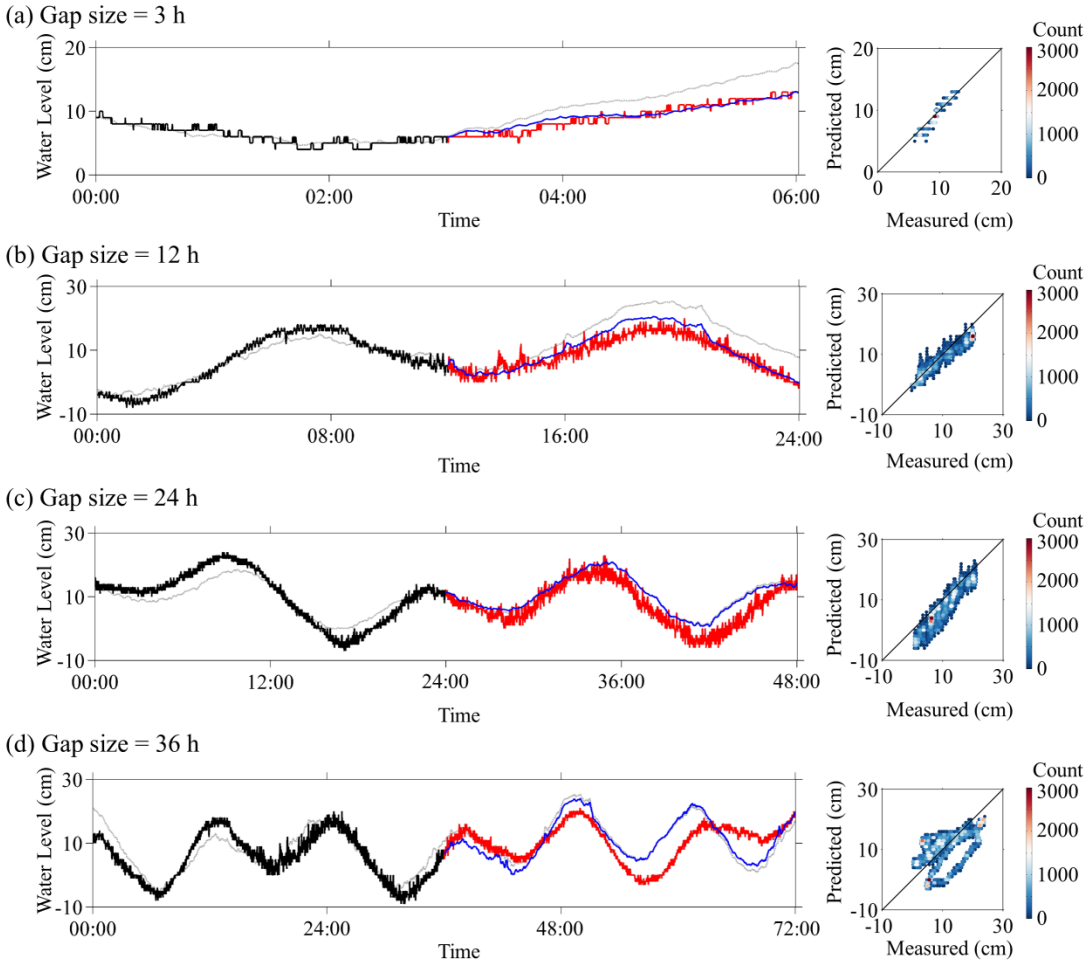

Figure 9: Examples of the gap filling algorithm using the calibrated parameters when the gap sizes are: (a) 3 h, (b) 12 h, (c) 24 h, and (d) 36 h. The left panel shows the time-series. The black lines represent the target data, and the gray lines represent the data of the selected search window. Blue lines represent the SWEP data; Red lines represent the measured data that was intentionally omitted. The right panel shows the scatter plot between the predicted data (or the SWEP data) and the measured data. The color point represents the frequency of data plotted inside the circle with a radius of 1 cm.

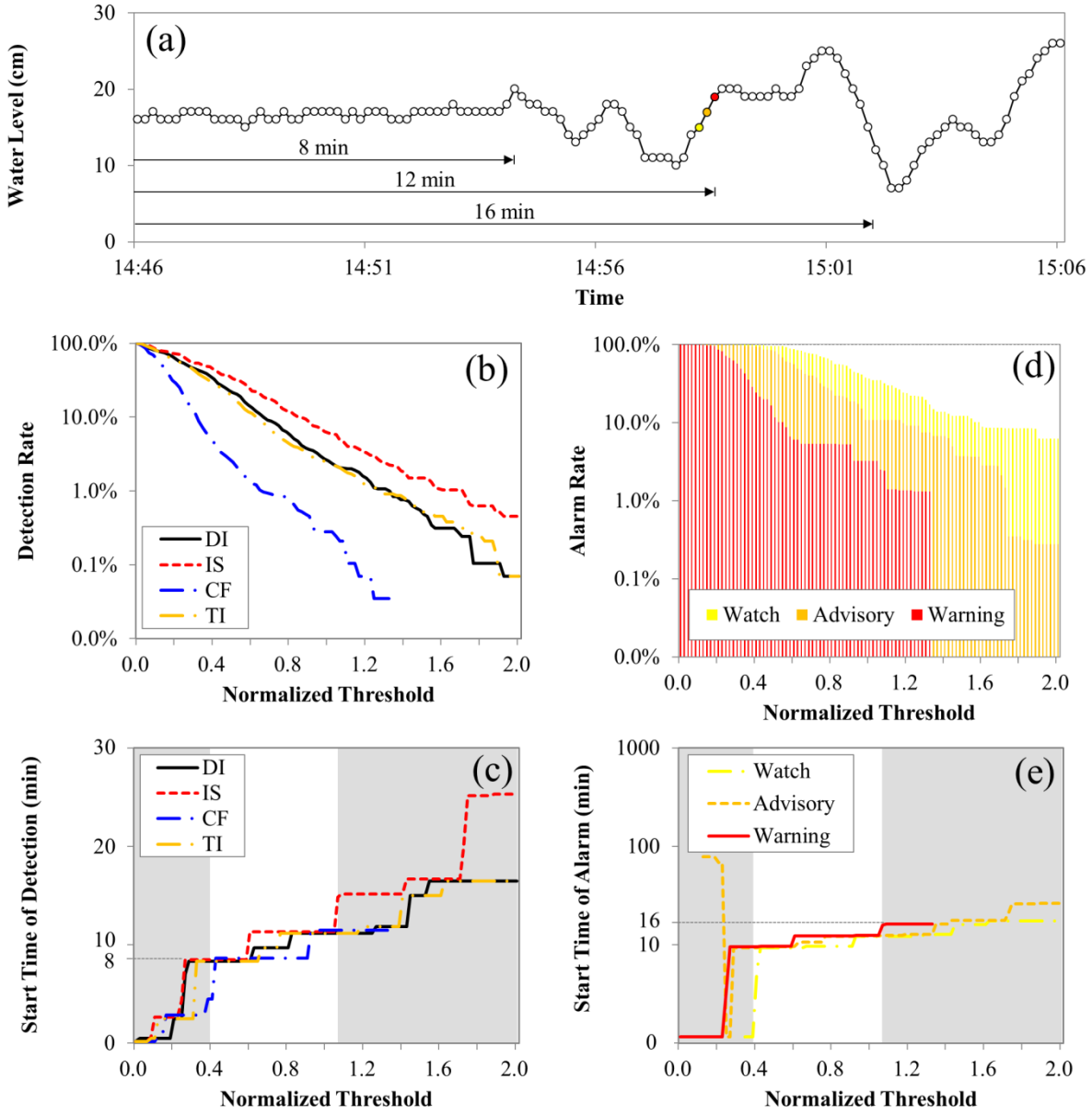

Figure 10: Examples of the tsunami detection algorithm using the calibrated parameters when the normalized threshold changes from 0 to 2 with 0.02 intervals. (a) The 2011 Tohoku tsunami recorded in the Ulleung-do surge gauge. The colored circle represents the start point of each alarm (red: warning, orange: advisory, yellow: watch) when the normalized threshold is set to one (TH_{DART} = 5 cm, TH_{IS} = 0.01 cm/s, TH_{CF} = 4, TH_{TIDE} = 5 cm). For each index (DI, IS, CF and TI), (b) detection rate during the event period and (c) start time of detection are given. For each alarm (warning, advisory and watch), (d) alarm rate during the event period and (e) start time of alarm are given. The gray shade region marks the range of the normalized threshold where a false or missed alarm occurs.

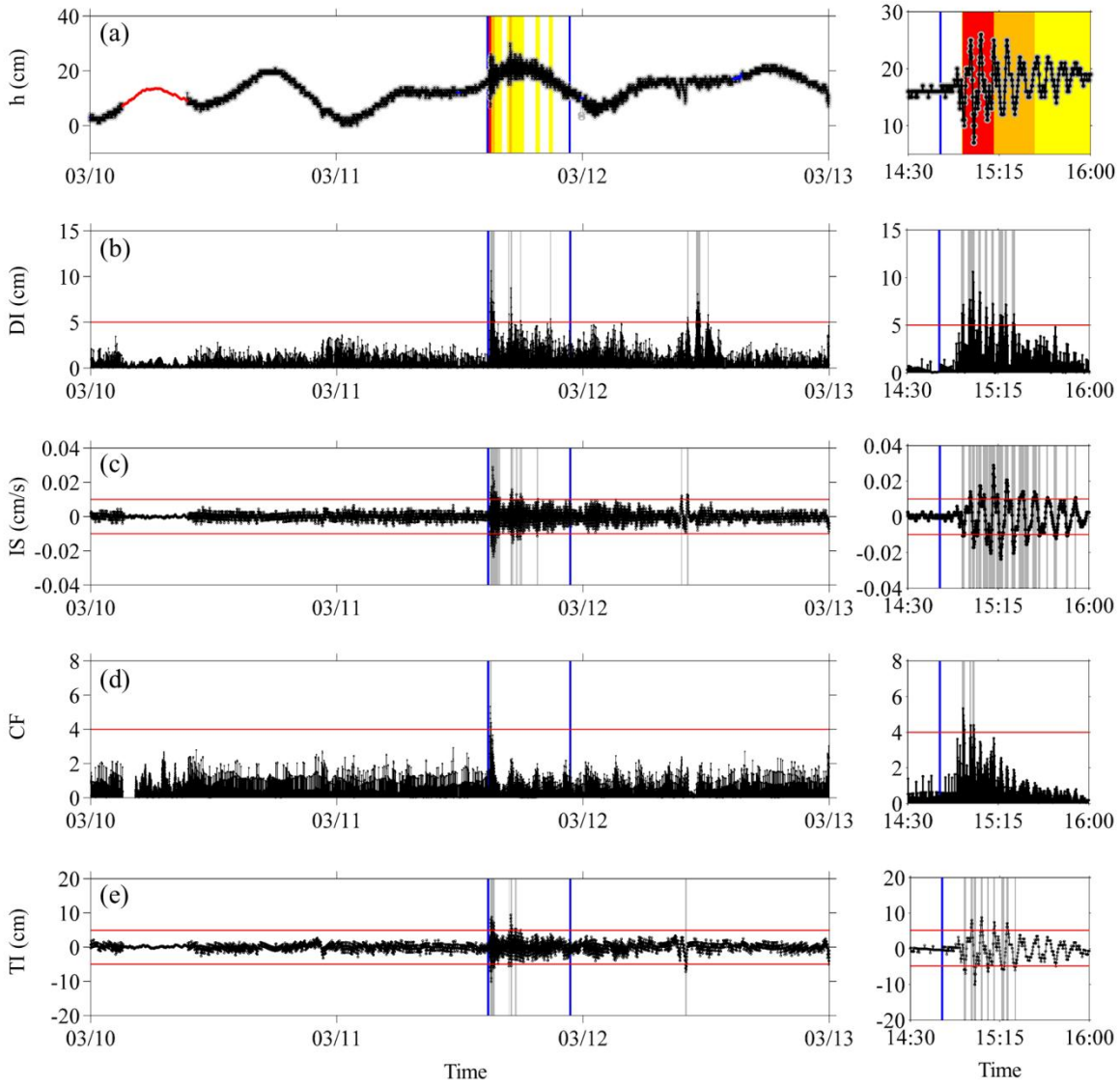

Figure 11: Performance test of TADS for the case of the 2011 Tohoku tsunami. Blue vertical lines show the event period from March 11 14:46 to March 11 22:46. For clarity, the records near the tsunami arrival time are zoomed in the right side. (a) Time-series of the Ulleung-do surge gauge after applying the TADS (black line) where outliers are marked by a gray line and gap-filled data are marked by a blue line (SGFA) and red line (LGFA). Vertical lines represent the alarm: warning (red), advisory (orange) and watch (yellow). Four indices of the tsunami detection algorithm are given: (b) DI, (c) IS, (d) CF and (e) TI. Red horizontal lines represent the thresholds and gray vertical lines mark the time whenever thresholds are triggered.

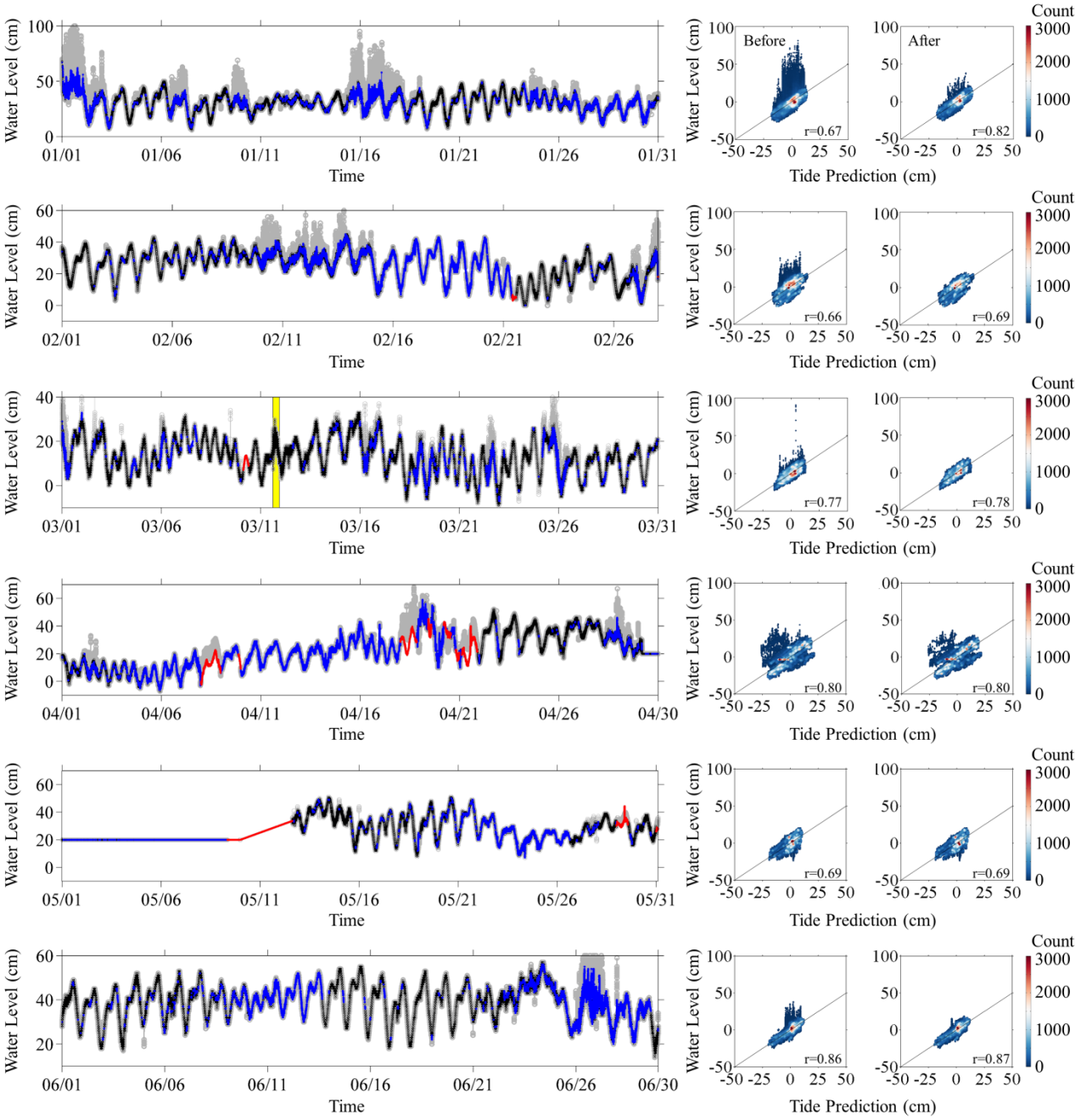

Figure 12: Performance test of the outlier removal and gap filling algorithms. (Left) Time-series of the Ulleung-do surge gauge after applying both outlier removal and gap filling algorithms (black line). Outliers are marked by a gray line and gap-filled data are marked by a blue line (SGFA) and a red line (LGFA). The yellow box in March indicates the event period. (Middle and right) Scatter plots show the comparison between before and after applying both outlier removal and gap filling algorithms. The mean value of each axis in the scatter plot is fixed to 0 by subtracting the mean value of each data from its data. The color point represents the frequency of data plotted inside the circle with a radius of 1 cm. The right corner represents the correlation coefficients.

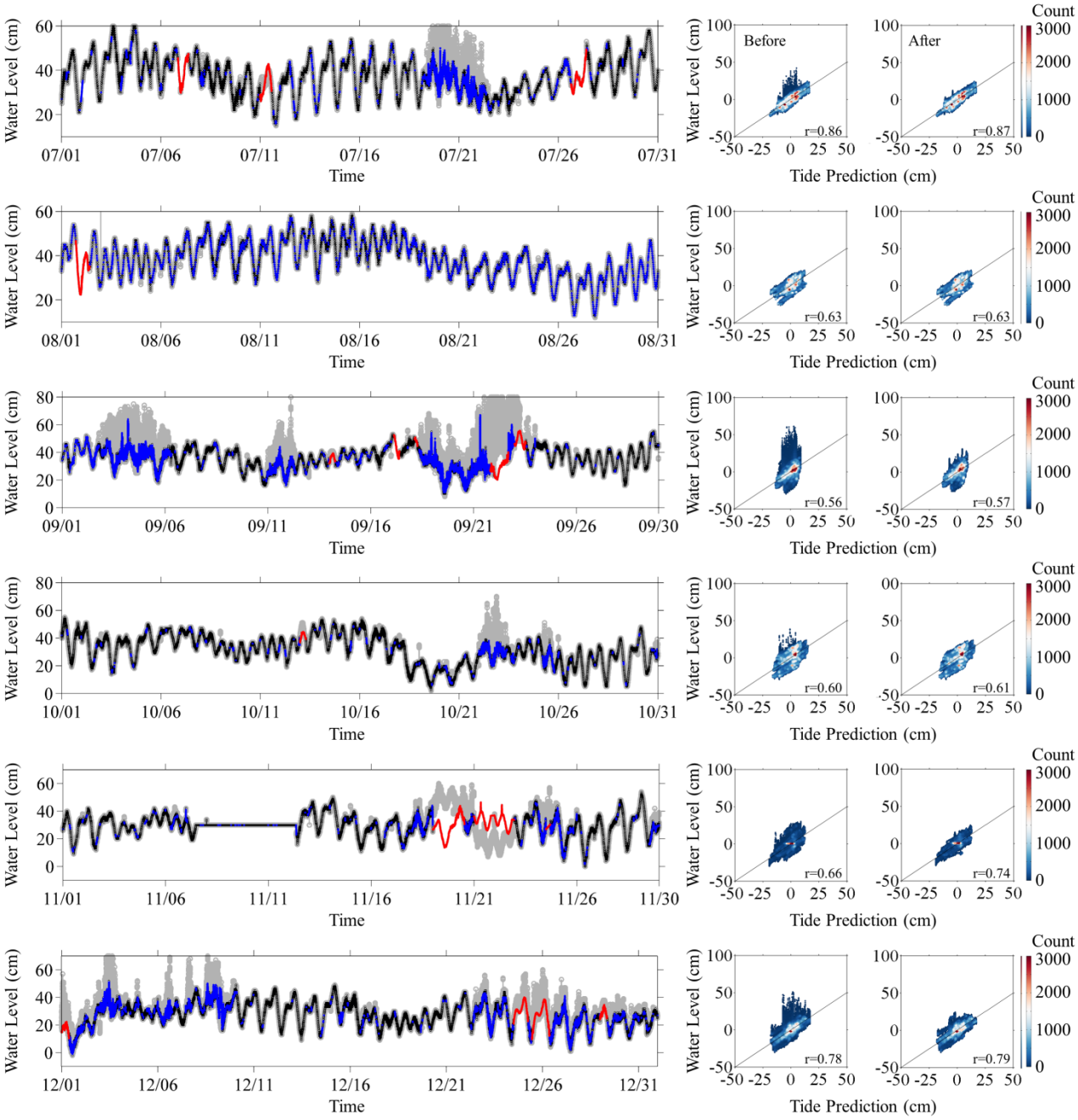

Figure 12: Continued.

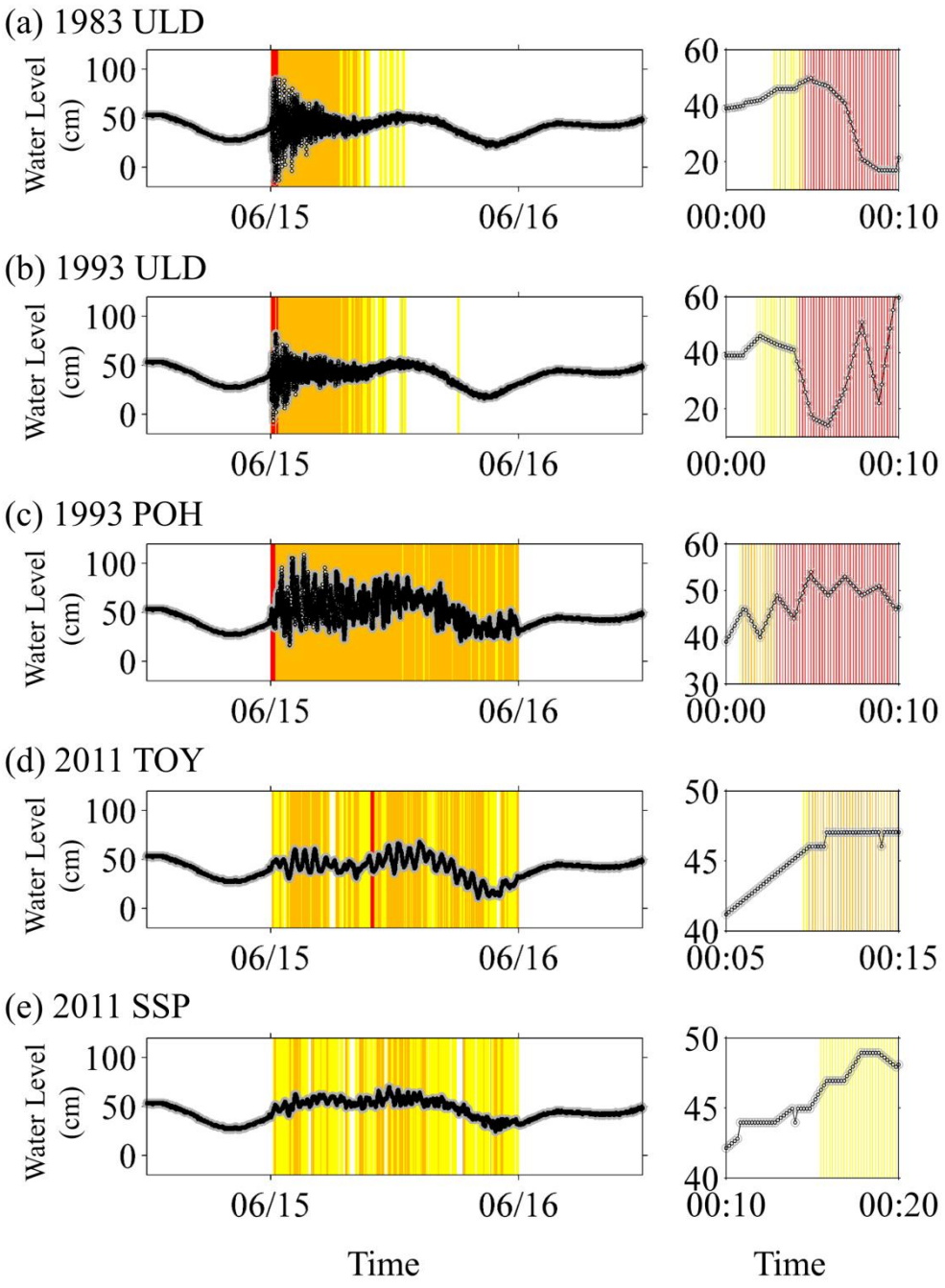

Figure 13: Synthetic tsunami records combining the records of tide stations with the background records of the Ulleung-do surge gauge: (a) 1983 ULD (Ulleung-do), (b) 1993 ULD (Ulleung-do), (c) 1993 POH (Pohang), (d) 2011 TOY (Tongyeong) and (e) 2011 SSP (Seongsanpo). For clarity, the records near the tsunami arrival time are zoomed in the right side. The arrival time is fixed to June 15, 2011, and the event period is set to 24 hours. Vertical lines represent the alarm: warning (red), advisory (orange) and watch (yellow).

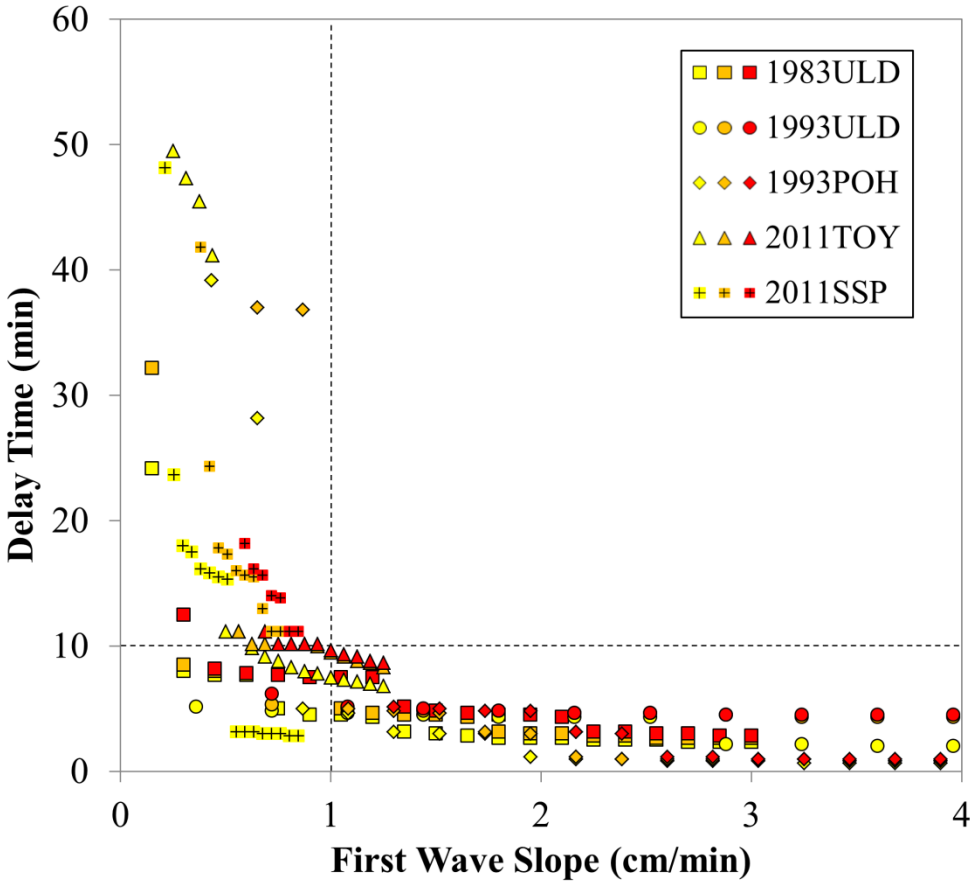

Figure 14: Performance test of the tsunami detection algorithm. The delay times are depicted distinctly depending on the types of synthetic tsunamis: 1983 ULD (rectangle), 1993ULD (circle), 1993POH (diamond), 2011TOY (triangle) and 2011SSP (cross). The types of alarms are depicted distinctly: warning (red), advisory (orange) and watch (yellow).